J Physiol 589.13 (2011) pp 3191–3209

The Journal of Physiology

Disruption of metabotropic glutamate receptor signalling is a major defect at cerebellar parallel fibre–Purkinje cell synapses in *staggerer* mutant mice

Kazuhiro Mitsumura[1,2], Nobutake Hosoi[1], Nobuhiko Furuya[2] and Hirokazu Hirai[1]

[1]*Department of Neurophysiology, Gunma University Graduate School of Medicine, Maebashi, Gunma 371-8511, Japan*
[2]*Department of Otolaryngology – Head and Neck Surgery, Gunma University Graduate School of Medicine, Gunma 371-8511, Japan*

Non-technical summary Homozygous *staggerer* mutant (*sg*/*sg*) mice exhibit cerebellar atrophy and congenital ataxia, and serve as an important extreme mouse model of the hereditary spinocerebellar ataxia type 1 (SCA1), since the *staggerer* mutation is closely related to SCA1 pathology. However, we know little about synaptic abnormalities at cerebellar parallel fibre (PF)–Purkinje cell (PC) synapses in *sg*/*sg* mice, which could underlie SCA1 pathology. In this study, we report that PFs still make reasonably functional fast synapses onto PCs in *sg*/*sg* mice despite reduction in the number of PF–PC synapses. In contrast, *sg*/*sg* mice lack metabotropic glutamate receptor (mGluR)-mediated slow synaptic transmission completely. Synaptic modulation caused by mGluR-mediated endocannabinoid release is also abolished at *sg*/*sg* PF–PC synapses. Our results indicate that major synaptic abnormality is disruption of cerebellar mGluR signalling in SCA1-related *sg*/*sg* mice, and that mGluR signalling can be one of the key factors to SCA1 pathology.

Abstract *Staggerer* mutant mice have functional loss of a transcription factor, retinoid-related orphan receptor α (RORα), which is abundantly expressed in Purkinje cells (PCs) of the cerebellum. Homozygous *staggerer* (*sg*/*sg*) mice show cerebellar hypoplasia and congenital ataxia. *Sg*/*sg* mice serve as an important extreme mouse model of the hereditary spinocerebellar ataxia type 1 (SCA1), since it has been shown that RORα dysfunction is strongly correlated with SCA1 pathogenesis. However, synaptic abnormalities, especially at parallel fibre (PF)–PC synapses, in SCA1-related *sg*/*sg* mice have not been examined in detail electrophysiologically. In this study, we report that PFs can still establish functional synapses onto PCs in *sg*/*sg* mice in spite of reduction in the number of PF–PC synapses. Compared with PF-evoked EPSCs in the wild-type or heterozygotes, the success rate of the EPSC recordings in *sg*/*sg* was quite low (~40%) and the EPSCs showed faster kinetics and slightly decreased paired pulse facilitation at short intervals. The prominent synaptic dysfunction is that *sg*/*sg* mice lack metabotropic glutamate receptor (mGluR)-mediated slow EPSCs completely. Neither intense PF stimulation nor an exogenously applied mGluR agonist, DHPG, could elicit mGluR-mediated responses. Western blot analysis in the *sg*/*sg* cerebellum revealed low-level expression of mGluR1 and TRPC3, both of which underlie mGluR-mediated slow currents in PCs. Immunohistochemical data demonstrated marked mislocalization of mGluR1 on *sg*/*sg* PCs. We found that mGluR-mediated retrograde suppression of PF–PC EPSCs by endocannabinoid is also impaired completely in *sg*/*sg* mice. These results suggest that disruption of mGluR signalling at PF–PC synapses is one of the major synaptic defects in *sg*/*sg* mice and may manifest itself in SCA1 pathology.

K. Mitsumura and N. Hosoi contributed equally to this work.

© 2011 The Authors. Journal compilation © 2011 The Physiological Society

DOI: 10.1113/jphysiol.2011.207563

(Received 21 February 2011; accepted after revision 3 May 2011; first published online 9 May 2011)
Corresponding author H. Hirai: Department of Neurophysiology, Gunma University Graduate School of Medicine, 3-39-22 Shouwamachi, Maebashi, Gunma 371-8511, Japan. Email: hiraih@med.gunma-u.ac.jp

Abbreviations AM251, a CB1 receptor antagonist; CAPS2, Ca^{2+}-dependent activator protein for secretion 2; Calbindin, calbindin D-28k; CB1, type 1 cannabinoid; DSE, depolarization-induced suppression of excitation; IP_3, inositol trisphosphate; ISI, interstimulus interval; mGluR, metabotropic glutamate receptor; PC, Purkinje cell; PF, parallel fibre; PPF, paired-pulse facilitation; PTP, post-tetanic potentiation; RORα, retinoid-related orphan receptor α; SCA1, spinocerebellar ataxia type 1; +/*sg*, heterozygous *staggerer* mutant; *sg*/*sg*, homozygous *staggerer* mutant; SSE, synaptically evoked suppression of excitation; TRPC3, canonical transient receptor potential type 3; VGluT1, vesicular glutamate transporter 1.

Introduction

The *staggerer* mutation causes functional impairment of a transcription factor, retinoid-related orphan receptor α (RORα), which belongs to the nuclear receptor superfamily (Boukhtouche *et al.* 2006; Gold *et al.* 2007). In the cerebellum, RORα is expressed dominantly in Purkinje cells (PCs) from late embryonic stages, and at low levels in stellate and basket interneurons (Hamilton *et al.* 1996; Ino, 2004). The *staggerer* mutation has been identified as a 122-base-pair deletion within the ligand binding domain of the RORα gene (Hamilton *et al.* 1996). This mutation prevents translation of the ligand binding domain of RORα protein and consequently, leads to loss of any transcriptional activity of RORα (Boukhtouche *et al.* 2006). Homozygous *staggerer* (*sg*/*sg*) mutant mice display similar cerebellar abnormalities to RORα-null mice, suggesting that *staggerer* is a loss of function of the RORα gene (Steinmayr *et al.* 1998; Doulazmi *et al.* 2001).

Heterozygous *staggerer* (+/*sg*) mice seem normal at young adult age, except for age-dependent and sex-related cerebellar degenerative phenotypes (Boukhtouche *et al.* 2006; Gold *et al.* 2007), whereas *sg*/*sg* mice display severe congenital ataxia and cerebellar hypoplasia (Sidman *et al.* 1962). Morphologically, the *sg*/*sg* cerebellum is much smaller, the molecular layer is thinner, PCs are not arranged in a monolayer, and the dendritic arborization of PCs is rudimentary, not confined to a single plane and devoid of tertiary dendritic spines (Sotelo, 1990; Sotelo & Dusart, 2009). In *sg*/*sg* mice, most PCs degenerate cell-autonomously by 2 months of age (Doulazmi *et al.* 2001), whereas loss of granule cells also occurs indirectly because of intrinsic defects in *sg*/*sg* PCs (Herrup & Mullen, 1981). The surviving PCs (∼20%) (Herrup & Mullen, 1981; Doulazmi *et al.* 2001) can form synapses with climbing fibres, although they remain multiply innervated even at adult age because of a failure in the developmental elimination of surplus climbing fibres (Mariani & Changeux, 1980; Steinmayr *et al.* 1998). On the other hand, it has been reported that parallel fibres (PFs) cannot make mature spine-type functional synapses onto PCs in *sg*/*sg* mice (Hirano & Dembitzer, 1975; Sotelo, 1975, 1990; Landis & Reese, 1977; Berry *et al.* 1978; Janmaat *et al.* 2009); however, previous ultrastructural studies also showed that some PFs from remaining granule cells are able to form primitive synapse-like junctional structures on *sg*/*sg* PCs (Sotelo, 1973, 1975, 1990; Hirano & Dembitzer, 1975; Berry *et al.* 1978). It remains unclear whether such primitive junctions function as synapses since detailed electrophysiological investigation has not been performed on PF–PC synaptic transmission in *sg*/*sg* mice. Moreover, dysfunction of RORα is involved in the pathogenesis of spinocerebellar ataxia type 1 (SCA1), which is caused by abnormal polyglutamine repeat expansion of ataxin-1 (Serra *et al.* 2006). Thus, electrophysiological analysis of PF–PC synapses in *sg*/*sg* mice can help clarify the mechanisms of SCA1 pathogenesis as well as the functional roles of RORα.

In the present study, we examined the electrophysiological properties of PF–PC synapses in *sg*/*sg* mice by a slice patch-clamp technique. PFs in *sg*/*sg* mice were still able to establish functional synapses onto PCs although the number of synapses was substantially reduced. In sharp contrast to wild-type (WT) or +/*sg* mice, *sg*/*sg* mice lacked mGluR1-mediated signalling completely. Disruption of mGluR1 signalling is a major synaptic abnormality in *sg*/*sg* mice and may underlie SCA1 pathogenesis.

Methods

Ethical approval

Staggerer mutant mice (kindly provided by Noriyuki Koibuchi, Gunma University Graduate School of Medicine) were maintained on a C57BL/6J genetic background in our breeding colony at the Institute of Experimental Animal Research, Gunma University Graduate School of Medicine. Homozygous *staggerer* (*sg*/*sg*), heterozygous *staggerer* (+/*sg*) and wild-type (WT) mice were bred from intercrossing fertile heterozygotes (Qiu *et al.* 2007). Genotypes of the mice were confirmed by PCR amplification of genomic DNA (Qiu *et al.*

© 2011 The Authors. Journal compilation © 2011 The Physiological Society

2007). Young adult mice (postnatal day 21–25) were used for all the experiments in this study. All the procedures for the care and treatment of the animals were carried out according to the Japanese Act on the Welfare and Management of Animals, and Guidelines for Proper Conduct of Animal Experiments issued by the Science Council of Japan. All the experimental protocols were approved by Gunma University Animal Care and Experimental Committee, and comply with *The Journal of Physiology* policy (Drummond, 2009) and UK regulations on animal studies.

Electrophysiology

Parasagittal cerebellar slices (200–250 μm in thickness) were prepared from 21- to 25-day-old mice as described previously (Llano *et al.* 1991) with minor modifications. Briefly, mice were anaesthetized deeply with inhalation of isoflurane (3%) and killed by decapitation. The whole brain was quickly dissected out and immersed for a couple of minutes in an ice-cold solution containing the following (in mM): 234 sucrose, 26 $NaHCO_3$, 2.5 KCl, 1.25 NaH_2PO_4, 11 glucose, 10 $MgSO_4$, 0.5 $CaCl_2$ (pH 7.4 when bubbled with 95% O_2 and 5% CO_2). Parasagittal slices of the cerebellar vermis were obtained using a microslicer (ZERO1; Dosaka-EM, Kyoto, Japan). The slices were maintained in an extracellular solution containing (in mM): 125 NaCl, 2.5 KCl, 2 $CaCl_2$, 1 $MgCl_2$, 1.25 NaH_2PO_4, 26 $NaHCO_3$, 10 D-glucose, and 0.1 picrotoxin, bubbled continuously with a mixture of 95% O_2 and 5% CO_2 at room temperature for at least 45 min before the beginning of recordings. PCs were visualized using a 40× water-immersion objective attached to an upright microscope (Axioskop; Zeiss, Germany). All whole-cell recordings were made from PCs at room temperature (26°C) and the slices were continuously perfused with the extracellular solution during the experiment. The resistance of patch pipettes was 3–4 MΩ when filled with intracellular solution containing (in mM): 65 potassium gluconate, 65 caesium methanesulfonate, 10 KCl, 1 $MgCl_2$, 4 Na_2ATP, 1 NaGTP, 20 Hepes, 0.4 EGTA and 5 sucrose (pH 7.3, adjusted with CsOH). In some experiments, 0.5% biocytin (w/v) was included in the intracellular solution to examine PC morphology. After the recording session, the slice was immersed in 4% paraformaldehyde dissolved in 0.1 M phosphate buffer and fixed at 4°C for at least 12 h. Biocytin-filled PCs were visualized by incubating the slice at room temperature for 2–3 h in a phosphate buffer solution containing 2% bovine serum albumin, 2% normal goat serum, 0.4% Triton X-100 and streptavidin-conjugated Alexa 594 (2 μg ml^{-1}; Invitrogen, Carlsbad, CA, USA).

Stimulation pipettes (5–10 μm tip diameter) were filled with the extracellular solution and placed in the molecular layer or in the granule cell layer to activate PFs or climbing fibres, respectively. Square pulses were applied for 100 μs with amplitudes ranging from 5 to 100 μA to elicit EPSCs in PCs. The holding potential of PCs was −70 mV, except when PCs were voltage-clamped at −10 mV for measuring climbing fibre-evoked EPSCs. Liquid junction potentials were not corrected. To estimate passive electrical properties of the recorded PCs, we applied 10 mV hyperpolarizing voltage pulses (from −70 mV to −80 mV, 200 ms duration). The averaged trace of 10 current responses was used for the estimation. Membrane capacitance and input resistance were calculated from the integral of the capacitive charging current, and from the steady-state current amplitude measured late during the pulse, respectively.

Selective stimulation of PFs was confirmed by paired-pulse facilitation (PPF) of EPSC amplitudes with a 50 ms or shorter interstimulus interval (ISI) and graded nature of the evoked EPSC amplitudes with the stimulus intensity (Konnerth *et al.* 1990; Perkel *et al.* 1990). To isolate mGluR1-mediated slow EPSCs, repetitive PF stimuli (100 Hz) were applied in the presence of 20 μM 2,3-dioxo-6-nitro-1,2,3,4-tetrahydrobenzo[f]quinoxaline-7-sulfonamide (NBQX). To measure agonist-induced mGluR1-mediated currents, (*S*)-3,5-dihydroxyphenylglycine (DHPG), a selective agonist for group I mGluRs (mGluR1 and mGluR5) was bath-applied at a flow rate of ∼2 ml min^{-1}. Cerebellar PCs express mGluR1 but not mGluR5 (Knopfel & Grandes, 2002; Ferraguti & Shigemoto, 2006), and thus DHPG-induced currents in PCs are considered to be mediated by mGluR1. Because of the large volume of the recording chamber (∼3 ml), solution exchange was relatively slow and the onset and kinetics of DHPG-induced currents were variable (Fig. 7). This was also the case with AMPA receptor agonist-induced currents, when (*RS*)-α-amino-3-hydroxy-5-methyl-4-isoxazolepropionic acid (*RS*-AMPA) was applied in the same way as DHPG, except in the presence of 1 μM tetrodotoxin, 100 μM cyclothiazide and 100 μM $CdCl_2$ to prevent the activation of voltage-gated sodium channels, AMPA receptor desensitization and synaptically evoked responses, respectively (Supplemental Fig. S1). This variation might depend on the location of the recorded cells in the chamber. Since the bath-applied agonist-induced responses developed slowly and spontaneous EPSCs were sometimes observed (Fig. 7), peak amplitudes of the agonist-induced currents were defined as averaged values during the current 50 ms before and after the peak time point, in order to minimize the contribution of randomly occurring spontaneous EPSCs superimposed on the response. The baseline amplitudes for measurement of the peak were defined as mean current amplitudes during 100 ms before the agonist solution reached the recording chamber (Fig. 7*A*, arrows and supplemental Fig. S1*A*,

© 2011 The Authors. Journal compilation © 2011 The Physiological Society

arrows). *N*-(piperidin-1-yl)-5-(4-iodophenyl)-1-(2,4-dichlorophenyl)-4-methyl-1*H*-pyrazole-3-carboxamide (AM251), 7-hydroxyiminocyclopropan[b]chromen-1a-carboxylate ethyl ester (CPCCOEt), NBQX, *RS*-AMPA and picrotoxin were obtained from Tocris Bioscience (Ellisville, MO, USA).

An EPC-8 amplifier (HEKA Elektronik, Lambrecht/Pfalz, Germany) and pCLAMP9 software (Molecular Devices, Sunnyvale, CA, USA) were used for recordings and data analysis. Some data were analysed with Igor Pro (Wavemetrics) using NeuroMatic software (http://www.neuromatic.thinkrandom.com/). The signals were filtered at 3 kHz and digitized at 10 kHz (Digidata 1322A; Molecular Devices).

Immunohistochemistry and morphological analysis

Mice were perfused transcardially with a fixative containing 4% paraformaldehyde in 0.1 M phosphate buffer after being anaesthetized deeply with sodium pentobarbital (40 mg (kg body weight)$^{-1}$). The whole brain was removed and postfixed in the same fixative overnight. The cerebellar vermis was then cut into 50 μm sagittal sections using a microslicer (Dosaka DTK-1000; Kyoto, Japan). The slices were incubated with phosphate-buffered saline (PBS) containing 10% donkey serum, 10% normal goat serum, and 0.1% Triton X-100 for 20 min at room temperature. For immunohistochemical staining, free-floating slices were treated with PBS containing 0.1% Triton X-100 and mixtures of primary antibodies overnight at room temperature. The mixtures contained mouse monoclonal anti-calbindin D-28K (1:500; Swant, Bellinzona, Switzerland), guinea pig polyclonal anti-VGluT1 (1:200; Frontier Institute, Ishikari, Japan), and either rabbit polyclonal anti-GluR2 N terminus (Matsuda *et al.* 1999) (1:500; Fig. 3) or rabbit polyclonal anti-mGluR1α (1:200; Frontier Institute; Fig. 6) antibodies. After tissue sections were washed in PBS, bound primary antibodies were detected by DyLight Fluor 488-conjugated donkey anti-guinea pig IgG (1:200; Jackson ImmunoResearch Laboratories, West Grove, PA, USA), Alexa Fluor 568-conjugated goat anti-rabbit IgG (1:200; Invitrogen) and Alexa Fluor 680-conjugated goat anti-mouse IgG (1:200; Invitrogen) antibodies dissolved in PBS and 0.1% Triton X-100. The sections were immunoreacted for 2–3 h at room temperature. To detect the distribution of TRPC3 (Fig. 7*D*), free-floating sections were treated with mouse monoclonal anti-calbindin D-28K (1:500) and rabbit polyclonal anti-TRPC3 (1:200; Alomone Labs, Jerusalem, Israel) antibodies with two overnight incubations at 4°C. The antibody diluent was a phosphate buffer containing 2% bovine serum albumin, 2% normal goat serum, and 0.4% Triton X-100. The immuno-positive signals were visualized by Alexa Fluor 488-conjugated goat anti-rabbit IgG (1:1000; Invitrogen) and Alexa Fluor 568-conjugated goat anti-mouse IgG (1:1000; Invitrogen) antibodies.

Fluorescence images of the stained slices and the biocytin-infused PCs were obtained using a confocal laser-scanning microscope (LSM 5 Pascal; Zeiss, Germany). To measure morphological parameters of the PCs (Fig. 1), a three-dimensional structure of each PC was reconstructed from ~40 z-stack images (1 μm optical depth) and analysed with Zeiss LSM Image Browser software (Zeiss, Germany). The width of PC arborization was defined as the maximal width of the arborization area in the sagittal plane (Fig. 1*B*, Sagittal view). The width was measured along a line perpendicular to the longitudinal axis of each PC, which is readily recognized as a parallel axis to the primary dendrite of PCs or to the axon descending to the granule cell layer. Axial length was determined as the maximal length of the arborization area, which was measured along the longitudinal axis from the root of the primary dendrite or the opposite pole of the axonal origin. To measure the depth of arborization, the reconstructed structure was rotated to the coronal plane (Fig. 1*B*, Coronal view). We defined the depth of arborization as the maximal length of the arborization area in the coronal plane. The depth was measured vertically to the longitudinal axis. In *sg*/*sg* mice, PC arborization is not flat on a single plane (Landis & Sidman, 1978) (Fig. 1*B*), and thus the coronal plane was defined as a plane where the depth of arborization was minimal in the reconstructed structure. The sagittal plane in *sg*/*sg* PCs was also defined as a plane where the width of arborization was maximal.

Western blot analysis

Cerebellar vermes from the genotyped mice were homogenized and solubilized in lysis buffer containing 50% PBS (v/v), 5 mM EDTA and 1% Triton X-100 supplemented with a cocktail of protease inhibitors (Nacalai Tesque, Kyoto, Japan). After sonication and centrifugation (at ~16,000× *g* for 20 min at 4°C) of the lysates, total protein concentration of the supernatants was determined using an NIPA kit (Non-Interfering Protein Assay; Calbiochem, Darmstadt, Germany). The samples were incubated for 15 min at 37°C in the presence of 2% sodium dodecyl sulfate (SDS), 10% glycerol, 50 mM DTT and 62.5 mM Tris-Cl (pH 6.8), and then electrophoresed on SDS polyacrylamide gels (7.5%) and transferred to PVDF membranes (Immobilon; Millipore, Billerica, MA, USA). The membranes were blocked with 5% non-fat skimmed milk in Tris-buffered saline (TBS) containing 0.2% Tween-20. Immunoreaction was performed with rabbit polyclonal anti-mGluR1α (1:5000), anti-GluR2/3 (1:1000; Chemicon, Temecula, CA, USA), anti-TRPC3 (1:3000) or mouse polyclonal anti-β-actin (1:10000; Sigma)

© 2011 The Authors. Journal compilation © 2011 The Physiological Society

antibodies. The secondary antibodies were HRP-conjugated anti-rabbit or anti-mouse IgG (Bio-Rad, Tokyo, Japan) at 1:25000 dilution. The antibodies were solubilized in Can Get Signal immunoreactions enhancer solution (Toyobo, Osaka, Japan) except the anti-β-actin antibody, which was diluted in TBS containing 0.2% Tween-20. Immunoreactive bands were visualized using an enhanced chemiluminescence reagent (ECL plus; GE Healthcare, Piscataway, NJ, USA). The amount of each expressed protein was quantified using ImageJ software (NIH, Bethesda, MD, USA) and normalized to the level of β-actin, a general house-keeping protein. Both the monomer and dimer of mGluR1 proteins were included to measure the amount of expressed mGluR1 (Zu *et al.* 2004). The membranes were probed repeatedly with different antibodies after stripping the antibodies from the membranes by incubating them for 30 min at 37°C in a commercially available stripping buffer (Restore Plus Western Blot Stripping Buffer; Thermo Scientific). All the results of immunoblot analysis were comparable to the results of mRNA expression revealed by quantitative rapid-cycle real-time RT-PCR (data not shown).

Statistics

Statistical tests were performed using the R software statistical package (www.r-project.org). When the data passed Bartlett's test of equal variance, Tukey's HSD *post hoc* test was used to compare all three groups to one another after one-way ANOVA; otherwise, the Steel–Dwass test was used for multiple comparisons after the Kruskal–Wallis test. For pairwise multiple comparisons in Fig. 2*B* (success rate of PF-evoked EPSC recordings), we used the Fisher's exact test followed by Holm's method. Differences were considered significant if $P < 0.05$. Pooled data are expressed as the mean ± SEM.

Results

In order to clarify the phenotypical difference between WT and *staggerer* mutant mice (+/*sg* and *sg*/*sg*) at PF–PC synapses, young adult (21- to 25-day-old) mice were used in the present study. At this age, the formation of PC dendrites and PF–PC synapses in WT mice are considered to be complete and mature (Hirano & Dembitzer, 1975; Puro & Woodward, 1977; Weiss & Pysh, 1978; McKay & Turner, 2005). In contrast, dendritic differentiation and spine formation of Purkinje cells in *sg*/*sg* mice remain severely retarded and immature at the corresponding age (Sotelo & Dusart, 2009). Together with the finding that most *sg*/*sg* mice die before P30 (Sidman *et al.* 1962), it is expected that we could efficiently examine *sg*/*sg* phenotypes at PF–PC synapses, using young adult mice in this study.

Passive electrical properties and morphological abnormalities in *staggerer* Purkinje cells

We first examined the passive electrical properties of PCs that might affect synaptic integration (Bekkers & Hausser, 2007) at PF–PC synapses in WT and *staggerer* mutant mice. Figure 1*A* shows membrane capacitance and input resistance measured by applying 10 mV hyperpolarizing voltage pulses to PCs in WT, +/*sg* and *sg*/*sg* mice. Membrane capacitance in *sg*/*sg* (89 ± 2 pF) was much smaller than in WT (567 ± 12 pF) or in +/*sg* (559 ± 11 pF) (Fig. 1*A*, left; Kruskal–Wallis test, $P < 0.0001$; WT *versus* *sg*/*sg*, $P < 0.0001$; +/*sg* *versus* *sg*/*sg*, $P < 0.0001$; WT *versus* +/*sg*, $P = 0.90$). Input resistance in *sg*/*sg* (192 ± 11 MΩ) was also significantly different from that in WT (119 ± 8 MΩ) or in +/*sg* (97 ± 5 MΩ), although a large variation was observed (Fig. 1*A*, right; Kruskal–Wallis test, $P < 0.0001$; WT *versus* *sg*/*sg*, $P < 0.0001$; +/*sg* *versus* *sg*/*sg*, $P < 0.0001$; WT *versus* +/*sg*, $P = 0.1$). The values of membrane capacitance and input resistance in WT and +/*sg* mice were comparable to those measured in previous studies (Hirai *et al.* 2003; Nakagami *et al.* 2008). We also confirmed aberrant arborization of PCs in *sg*/*sg* mice (Bradley & Berry, 1978; Landis & Sidman, 1978; Nakagawa *et al.* 1998) by visualizing PCs filled with biocytin via patch pipettes (Fig. 1*B*), while PCs in WT and +/*sg* mice exhibited normal morphological features (Fig. 1*B* and *C*; width of arborized region, WT 167.0 ± 7.1 μm, +/*sg* 143.3 ± 10.5 μm, *sg*/*sg* 95.0 ± 7.4 μm; ANOVA, $P < 0.0001$; WT *versus* *sg*/*sg*, $P < 0.0001$; +/*sg* *versus* *sg*/*sg*, $P < 0.01$; WT *versus* +/*sg*, $P = 0.12$: axial length of arborized region, WT 195.8 ± 14.6 μm, +/*sg* 189.3 ± 23.0 μm, *sg*/*sg* 57.1 ± 5.7 μm; Kruskal–Wallis test, $P < 0.0001$; WT *versus* *sg*/*sg*, $P < 0.0001$; +/*sg* *versus* *sg*/*sg*, $P < 0.0001$; WT *versus* +/*sg*, $P = 0.50$: depth of arborized region, WT 7.4 ± 0.5 μm, +/*sg* 7.1 ± 0.6 μm, *sg*/*sg* 15.4 ± 2.0 μm; Kruskal–Wallis test, $P < 0.001$; WT *versus* *sg*/*sg*, $P < 0.01$; +/*sg* *versus* *sg*/*sg*, $P < 0.01$; WT *versus* +/*sg*, $P = 0.97$). These morphological abnormalities would result in smaller membrane capacitance and slightly higher input resistance of *sg*/*sg* PCs because of the reduction in surface membrane area of PCs (Crepel *et al.* 1984).

Properties of PF-evoked AMPA-receptor-mediated EPSCs in *staggerer* PCs

It has been reported that PFs in *sg*/*sg* mice are able to establish a small number of immature junctional complexes onto PC dendrites morphologically, although those synaptic contacts scarcely develop into spine-shaped mature synapses (Hirano & Dembitzer, 1975; Sotelo, 1975, 1990; Landis & Reese, 1977; Berry *et al.* 1978; Janmaat *et al.* 2009). To assess the functional properties of such PF–PC synapses in *staggerer* mutant mice, we tried

© 2011 The Authors. Journal compilation © 2011 The Physiological Society

to record PF-evoked excitatory synaptic responses from voltage-clamped PCs (Fig. 2). We successfully observed PF-evoked EPSCs, which exhibited typical paired-pulse facilitation (PPF) at short intervals (Konnerth *et al.* 1990; Perkel *et al.* 1990), in *sg*/*sg* mutant mice (Fig. 2*A*, right). PF-evoked EPSCs were completely abolished by NBQX (data not shown), confirming that the EPSCs are mediated by AMPA receptors (Konnerth *et al.* 1990; Perkel *et al.* 1990). The success rate of the EPSC recordings in *sg*/*sg* mice was quite low (~40%; WT *versus* *sg*/*sg*, $P < 0.0001$; +/*sg* *versus* *sg*/*sg*, $P < 0.0001$), while there was almost no failure in WT or in +/*sg* mice (Fig. 2*B*). In addition, climbing fibre-evoked EPSCs were recorded at a high success rate (~84%) from *sg*/*sg* PCs (data not shown), which are still multiply innervated by climbing fibres even at young adult age (Crepel *et al.* 1980; Mariani & Changeux, 1980; Steinmayr *et al.* 1998). Thus, we can minimize the possibility that the slicing procedure may damage the *sg*/*sg* cerebellar nerve fibres, leading to a low encounter rate of PF-evoked EPSCs in *sg*/*sg* mice. Rather, the low rate would reflect the partial loss of PFs caused by progressive degeneration of granule cells in the *sg*/*sg* mutant cerebellum (Hirano & Dembitzer, 1975; Sotelo, 1990).

Kinetic analysis revealed that the time course of PF-evoked EPSCs was much faster in *sg*/*sg* mice than in WT or +/*sg* mice (Fig. 2*A* and *C*; time to peak; WT, 5.6 ± 0.1 ms, $n = 39$, 8 mice; +/*sg* 5.3 ± 0.2 ms. $n = 42$, 7 mice; *sg*/*sg*, 3.2 ± 0.1 ms, $n = 44$, 19 mice: Kruskal–Wallis test, $P < 0.0001$; WT *versus* *sg*/*sg*, $P < 0.0001$; +/*sg* *versus* *sg*/*sg*, $P < 0.0001$, WT *versus* +/*sg*, $P = 0.27$: Fig. 2*A* and *D*; decay time constant; WT, 10.5 ± 0.4 ms, $n = 39$, 8 mice; +/*sg*, 9.8 ± 0.4 ms, $n = 42$, 7 mice; *sg*/*sg*, 3.5 ± 0.1 ms, $n = 44$, 19 mice: Kruskal–Wallis test, $P < 0.0001$; WT *versus* *sg*/*sg*, $P < 0.0001$; +/*sg* *versus* *sg*/*sg*, $P < 0.0001$; WT *versus* +/*sg*, $P = 0.44$). This may be because *sg*/*sg* PCs are electrotonically more compact because of their smaller size and consequently, the evoked EPSCs are much less filtered by the cable properties of less-branched rudimentary dendrites (Fig. 1).

To examine the time course of PPF at PF–PC synapses in WT and mutant mice (Fig. 2*A*), we varied inter-stimulus intervals (ISIs) of the two pulses from 10 ms to 5 s. The amplitude of the second EPSC evoked

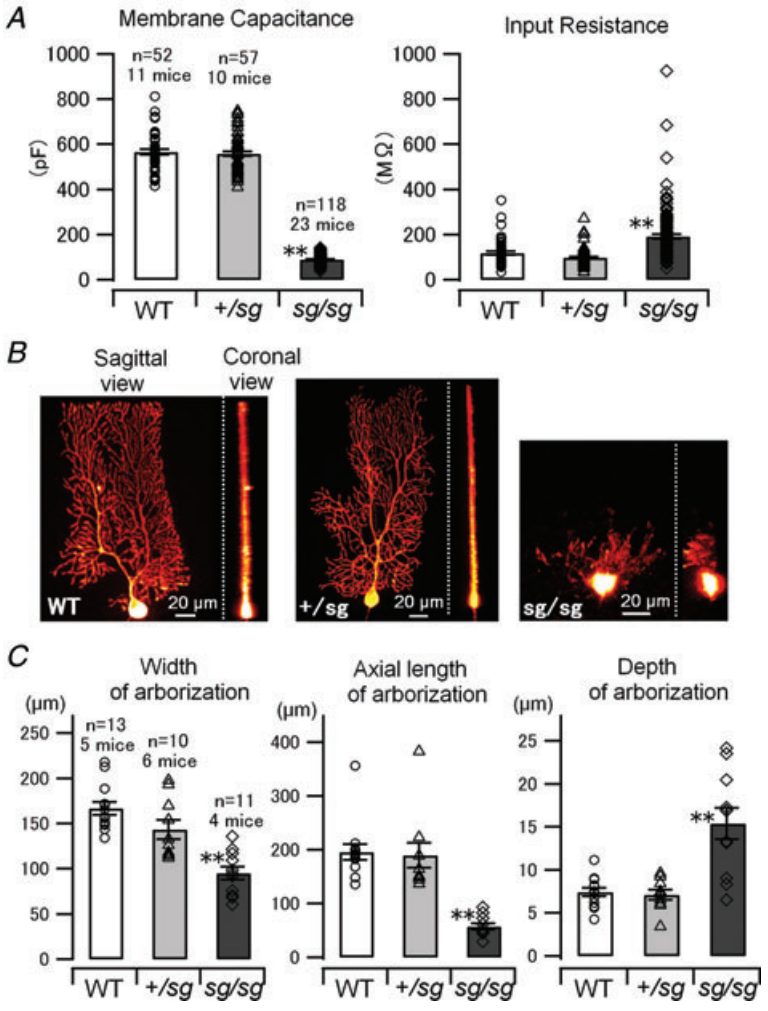

Figure 1. Passive electrical properties and aberrant morphology of PCs in *staggerer* mutant mice
A, membrane capacitance and input resistance of each PC (holding potential, −70 mV) was estimated from an averaged trace of 10 current responses elicited by 10 mV-hyperpolarizing voltage pulses (duration 200 ms). Symbols and bar graphs correspond to individual data points and mean values of the pooled data, respectively, in *A* (WT *versus* *sg*/*sg*, and +/*sg* *versus* *sg*/*sg*, $^{**}P < 0.0001$) and *C*. Error bars indicate SEM in this and subsequent figures. *B*, morphology of PCs revealed by biocytin infusion. Three-dimensional structures of PCs were reconstructed from tens of confocal z-stack images. Sagittal and coronal views of the reconstructed structures are shown. *C*, morphological parameters of PC arborization (Width, ANOVA, $P < 0.0001$; Axial length, Kruskal–Wallis test, $P < 0.0001$; Depth, Kruskal–Wallis test, $P < 0.001$: WT *versus* *sg*/*sg*, and +/*sg* *versus* *sg*/*sg*, $^{**}P < 0.01$) measured by the use of the reconstructed structures.

© 2011 The Authors. Journal compilation © 2011 The Physiological Society

by a stimulus pair was normalized to the one of the first EPSC, and the ratio (paired pulse ratio) was plotted against ISIs (Fig. 2*E*). There was no difference in the time course of facilitation between WT and +/*sg* mice (Fig. 2*E*, open circles and grey filled circles). However, *sg*/*sg* mice had significantly smaller degrees of facilitation at short intervals (Fig. 2*E*, black filled circles; ISI 20 ms, paired pulse ratio; WT 1.82 ± 0.06, +/*sg* 1.87 ± 0.04, *sg*/*sg* 1.57 ± 0.09; Kruskal–Wallis test, $P < 0.01$; WT *versus* *sg*/*sg*, $P < 0.05$; +/*sg* *versus* *sg*/*sg*, $P < 0.01$; WT *versus* +/*sg*, $P = 0.59$: ISI 50 ms, paired pulse ratio; WT 1.63 ± 0.05, +/*sg* 1.71 ± 0.04, *sg*/*sg* 1.49 ± 0.08; Kruskal–Wallis test, $P < 0.01$; +/*sg* *versus* *sg*/*sg*, $P < 0.01$; WT *versus* *sg*/*sg*, $P = 0.07$; WT *versus* +/*sg*, $P = 0.96$). This may reflect increased presynaptic release probability at *sg*/*sg* PF–PC synapses. Collectively, the above results indicate that PFs in *sg*/*sg* mice are able to establish functional synapses onto PCs and that the PF–PC synapses, however, have slightly altered short-term synaptic facilitation.

Morphological analysis of PF–PC synapse formation in *staggerer* mice

In order to examine how PF–PC synapses are formed in *staggerer* mutant mice, we visualized dendritic spines and putative synaptic sites in PCs by biocytin labelling and immunohistochemistry for synaptic proteins, respectively. Figure 3*A* shows the distribution of the dendritic spines on PCs in WT, +/*sg* and *sg*/*sg* mice. We observed numerous spines attached to the dendrites in WT and +/*sg* mice (Fig. 3*A*, left and middle), whereas the dendrites in *sg*/*sg* mice seemed smoother and had far fewer spines (Fig. 3*A*, right) as reported previously (Hirano & Dembitzer, 1975; Sotelo, 1975; Janmaat *et al.* 2009).

Figure 3*B*, *C* shows triple immunofluorescence for AMPA-type glutamate receptor subunit GluR2 (also known as GluRB or GluA2), vesicular glutamate transporter 1 (VGluT1) and calbindin D-28k (Calbindin) in the cerebellar cortex. Since Purkinje cells and other postsynaptic cells except Bergmann glia express GluR2-containing, Ca^{2+}-impermeable heteromeric

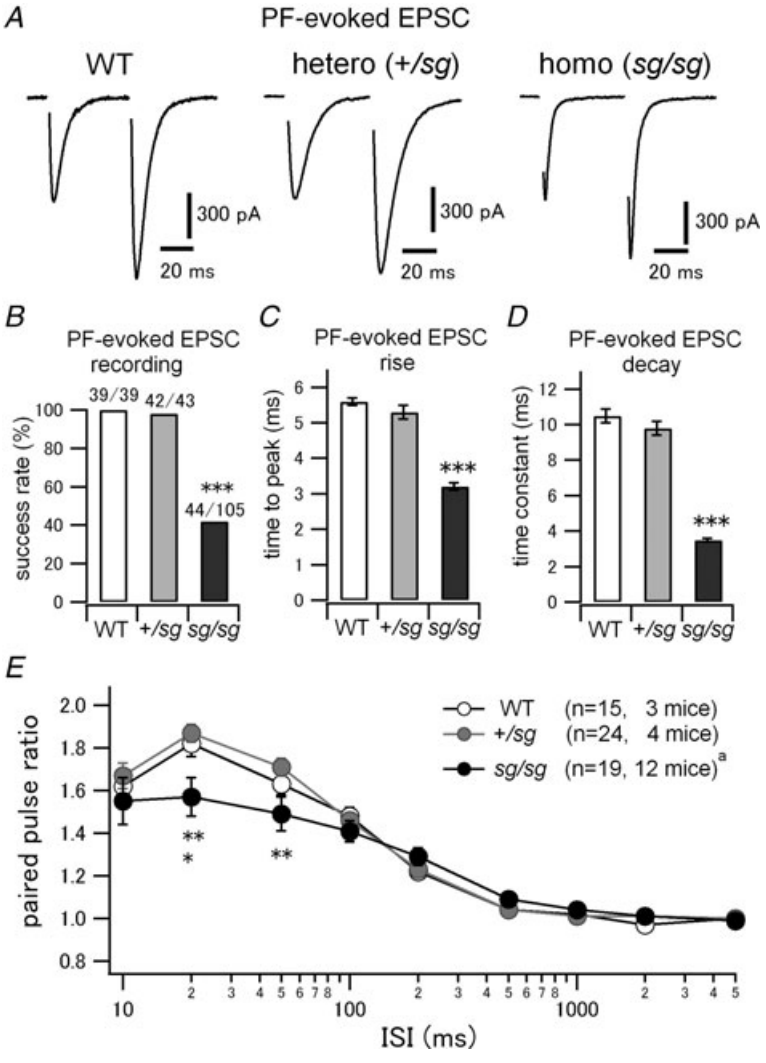

Figure 2. Some PF–PC synapses are functional but kinetics and short-term plasticity of PF-evoked EPSC are altered in *staggerer* mice
A, EPSCs were evoked by a paired pulse stimulation of PFs at an interval of 50 ms. Stimulus artifacts are blanked. PCs were voltage-clamped at −70 mV. The second EPSCs were facilitated, which is a typical nature of PF–PC synapses. *B*, rate of successful recordings of PF-evoked EPSCs in WT and *staggerer* mutants. Each denominator and numerator indicates the total number of tried cells and the number of cells where PF-evoked EPSCs were observed, respectively (WT *versus* *sg*/*sg* and +/*sg* *versus* *sg*/*sg*, $***P < 0.0001$). *C*, time from stimulus onset to peak of PF-evoked EPSCs (WT *versus* *sg*/*sg* and +/*sg* *versus* *sg*/*sg*, $***P < 0.0001$). *D*, decay time constants of PF-evoked EPSCs were measured by fitting a single exponential function. (WT *versus* *sg*/*sg* and +/*sg* *versus* *sg*/*sg*, *** $P < 0.0001$.) *E*, mean paired pulse ratios (the second EPSC amplitudes normalized to the first ones) were plotted against varied interstimulus intervals (ISIs) of the two pulses (WT *versus* *sg*/*sg*, $*P < 0.05$ and +/*sg* *versus* +/*sg*, $**P < 0.01$). [a]The sample size is different at ISI of 2 s ($n = 17$, 10 mice).

© 2011 The Authors. Journal compilation © 2011 The Physiological Society

AMPA receptors in the cerebellum (Burnashev *et al.* 1992; Sato *et al.* 1993), the immunofluorescence signal for GluR2 can be used as a postsynaptic marker at the glutamatergic synapses in the cerebellum. VGluT1 is a presynaptic marker selective for PF synapses in adult mice (Fremeau *et al.* 2001; Miyazaki *et al.* 2003). Calbindin D-28k is a Ca^{2+}-binding protein and a typical marker for PCs (Bastianelli, 2003). There was no discernable difference in the distribution of those proteins between WT and +/*sg* mice (Fig. 3*B* and *C*; left and middle rows). In *sg*/*sg* mice, punctate fluorescence signals from GluR2 and VGluT1 were larger and more sparsely distributed in the thinner molecular layer (Fig. 3*B* and *C*; right row) than in WT and in +/*sg* mice. In WT and +/*sg* mice, many GluR2-positive puncta (postsynaptic sites) were juxtaposed to, or overlapped with, the VGluT1-positive puncta (presynaptic sites) on the PC dendrites (Fig. 3*C*, bottom in left and middle rows, arrows). Meanwhile, in *sg*/*sg* mice, a much smaller number of GluR2-positive punctate signals were closely associated with VGluT1-positive signals at the smooth dendritic shafts lacking spines (Fig. 3*C*, right bottom, arrows), which is reminiscent of primitive junctions between PFs and PCs reported in previous ultrastructural studies (Sotelo, 1973, 1975, 1990; Hirano & Dembitzer, 1975; Berry *et al.* 1978). These results suggest that some, if not many, PFs make glutamatergic synaptic contacts onto the spine-less dendrites of PCs in *sg*/*sg* mutant mice. It should be noted that the number of putative synaptic contacts between PFs and PCs in *sg*/*sg* mice was much less than in WT and +/*sg* mice and that isolated GluR2-positive signals, which were not apposed to presynaptic VGluT1 signals, were sometimes observed on the dendritic shafts of *sg*/*sg* PCs (Fig. 3*C*, right bottom, arrowheads). These may also explain why the encounter rate of successful EPSC recordings is quite low at PF–PC synapses in *sg*/*sg* mice.

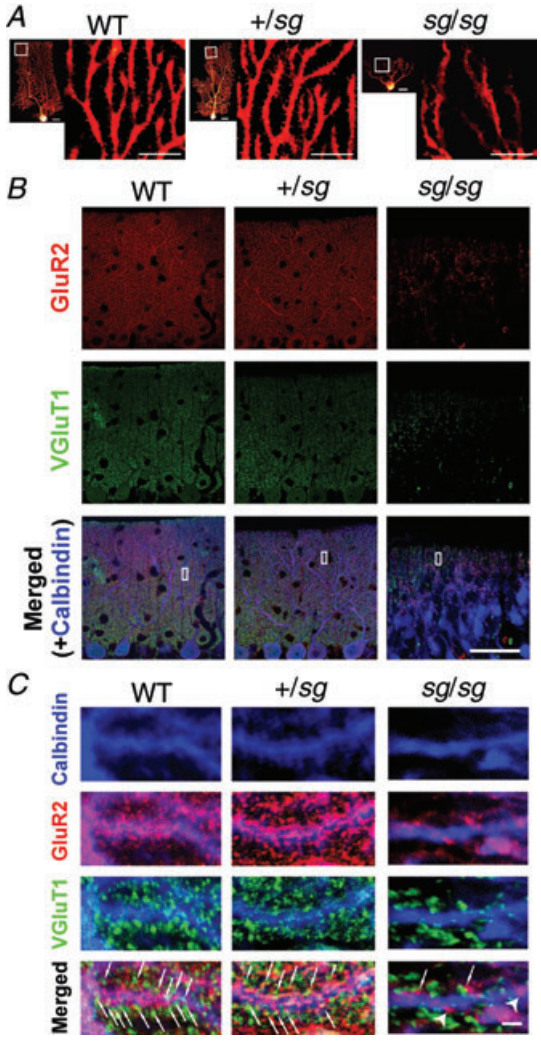

Figure 3. A small number of PF–PC synapses are formed onto spine-less dendrites of *sg*/*sg* PCs
A, distribution of dendritic spines visualized by introducing biocytin into PCs. Small images are overviews of the visualized PCs (scale bar, 20 μm). Each larger image (scale bar, 10 μm) shows a magnified view of the region marked by a white square in the left-neighbouring small image. *B* and *C*, confocal images of triple immunofluorescence for GluR2 (red; a postsynaptic marker), VGluT1 (green; a presynaptic marker for PF synapses) and Calbindin (blue; a marker for PCs). Left, middle and right rows correspond to the images obtained from WT, +/*sg* and *sg*/*sg* cerebellar slices, respectively. The regions specified by white rectangles in *B* are magnified and rotated in *C*. Arrows and arrowheads in *C* indicate putative synaptic sites and isolated postsynaptic sites without presynaptic partners on PCs, respectively. Scale bars represent 50 μm in *B* and 2 μm in *C*.

Lack of synaptically evoked mGluR-mediated slow EPSC in *staggerer* mice

At PF–PC synapses in the cerebellum, postsynaptic AMPA receptors mediates fast excitatory synaptic transmission, whereas perisynaptic mGluRs in PCs (Baude *et al.* 1993; Nusser *et al.* 1994) mediate slow electrical (Batchelor *et al.* 1994) and chemical responses (Finch & Augustine, 1998; Takechi *et al.* 1998), which are important for various synaptic plasticity, cerebellar development and motor coordination (Knopfel & Grandes, 2002; Nakao *et al.* 2007; Kano *et al.* 2008; Hartmann & Konnerth, 2009). Thus, we performed a series of experiments to examine mGluR signalling at PF–PC synapses in *sg*/*sg* mutant mice. First, we probed the properties of synaptically evoked mGluR-mediated slow EPSCs in WT and mutant mice. In order to isolate the mGluR-mediated EPSC component, the AMPA receptor antagonist NBQX (10–20 μM) was bath-applied. PFs were stimulated with brief high-frequency trains (5 pulses of PF stimulation at 100 Hz) at various stimulus intensities (0 to 100 μA), because the accumulation of synaptically released glutamate is essential to activate mGluRs located perisynaptically at PF–PC synapses (Baude *et al.* 1993;

© 2011 The Authors. Journal compilation © 2011 The Physiological Society

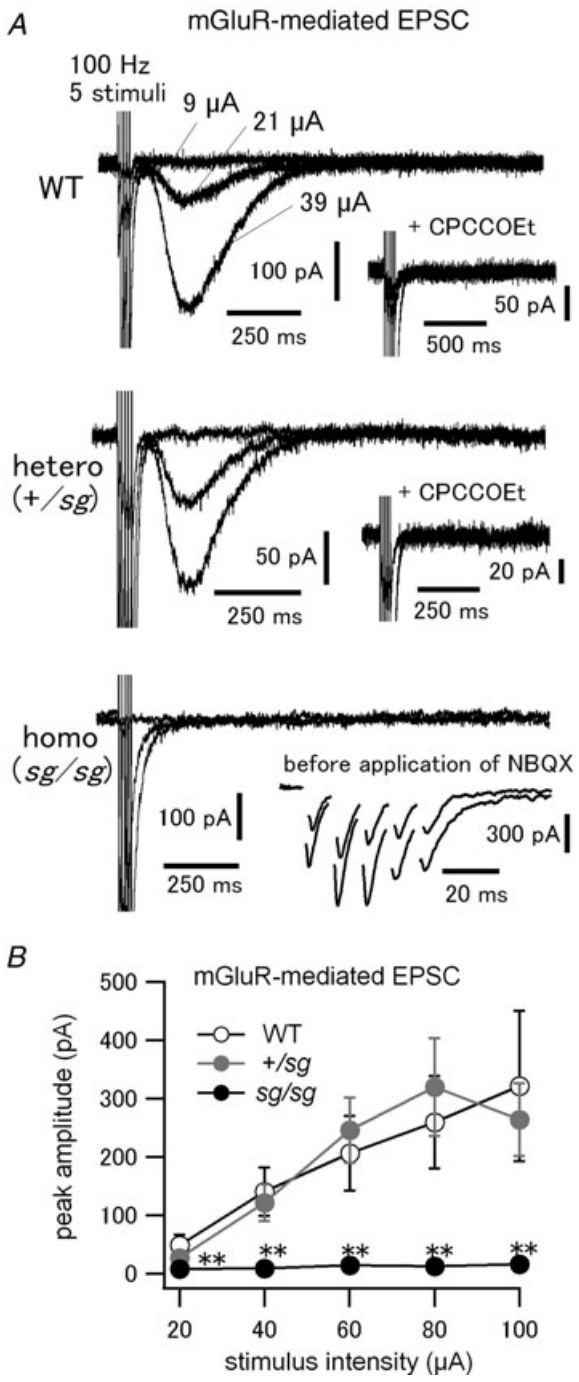

Figure 4. No mGluR-mediated slow EPSC in *sg*/*sg* PCs
A, brief PF burst stimulation (5 pulses at 100 Hz) was applied at varied stimulus intensities to evoke mGluR-mediated slow EPSCs in PCs. NBQX (10–20 μM) was included in the bath solution to block AMPA receptors and isolate mGluR-mediated EPSC. Three traces of the responses evoked at different stimulus intensities are shown. Stimulus intensities are specified only in the top panel. Insets in top and middle panels show abolition of the slow EPSCs after subsequent application of CPCCOEt (100 μM; a specific mGluR1 antagonist). Inset in bottom panel shows evoked AMPA receptor-mediated fast EPSCs recorded from the same cell before application of NBQX. *B*, pooled data of the relationship between stimulus intensities and peak amplitudes of mGluR-mediated slow EPSCs (WT *versus* *sg*/*sg* and +/*sg* *versus* *sg*/*sg*, $^{**}P < 0.01$ except at the stimulus intensity of 20 μA, where WT *versus* *sg*/*sg*, $P < 0.01$ and +/*sg* *versus* *sg*/*sg*, $P < 0.05$). The data at each stimulus intensity were obtained from 3–10 cells (3–8 mice).

Batchelor *et al.* 1994; Nusser *et al.* 1994; Tempia *et al.* 1998; Marcaggi & Attwell, 2005). The brief PF burst stimulation evoked slow EPSCs in WT and +/*sg* mice at stimulus intensities more than ~20 μA (Fig. 4*A*, top and middle). The peak amplitudes of slow EPSCs show monotonic increases in relation to the stimulus intensities, with no significant difference between WT and +/*sg* mice (Fig. 4*B*, open and grey filled circles). These slow currents were abolished by a selective mGluR1 antagonist, CPCCOEt (100 μM) (Fig. 4*A*, top and middle, inset), indicating that these currents were mediated by the activation of mGluR1 (Tempia *et al.* 1998; Canepari *et al.* 2001; Marcaggi & Attwell, 2005; Hartmann *et al.* 2008). Interestingly, mGluR-mediated slow EPSCs were never evoked by the brief PF burst stimulation in *sg*/*sg* mice (Fig. 4*A*, bottom), even at a strong stimulus intensity such as 100 μA (Fig. 4*B*, black filled circles). In all the tested *sg*/*sg* PCs, however, we confirmed the formation of synaptic contacts between PFs and PCs in advance, by observing AMPA receptor-mediated fast EPSCs before the application of NBQX (Fig. 4*A*, bottom, inset). Thus, we conclude that mGluR-mediated slow EPSCs are not induced by synaptically released glutamate at PF–PC synapses in *sg*/*sg* mice.

Western blot analysis and immunohistochemistry of mGluR1 in *staggerer* cerebellum

Among eight mGluR subtypes, mGluR1 is predominantly expressed in PCs and is thought to be involved in the generation of mGluR-mediated slow EPSCs in PCs (Knopfel & Grandes, 2002; Kano *et al.* 2008; Hartmann & Konnerth, 2009). To elucidate why mGluR-mediated slow EPSCs are not evoked by brief PF burst stimulation in *sg*/*sg* mice (Fig. 4), we examined the expression levels of mGluR1 in the cerebellar vermis of WT, +/*sg* and *sg*/*sg* mice, the same cerebellar region used for electrophysiological recordings in this study. Western blot analysis with normalization to the expression levels of β-actin, a general house-keeping protein, revealed that *sg*/*sg* mice express a markedly reduced level of mGluR1 including its monomer and dimer by ~85% of the level in WT (Kruskal–Wallis test, $P < 0.01$; WT *versus* *sg*/*sg*, $P < 0.01$) or heterozygous mice (+/*sg* *versus* *sg*/*sg*, $P < 0.05$) (Fig. 5*A*, top and 5*B*, grey bars). This is in line with previous reports that the mRNA level of mGluR1 is significantly reduced in *sg*/*sg* mice (Gold *et al.* 2003, 2007; Serra *et al.* 2006). The amount of

© 2011 The Authors. Journal compilation © 2011 The Physiological Society

mGluR1 expressed by +/*sg* mice was comparable to that by WT mice (Fig. 5*B*). It should be mentioned that the amount of GluR2/3 expressed by *sg*/*sg* mice was almost as little (∼30% of WT) as that of mGluR1 (Fig. 5*A*, middle and 5*B*, open bars), although the fast AMPA receptor-mediated EPSCs were successfully recorded in *sg*/*sg* mice, in contrast to mGluR-mediated slow EPSCs (Figs 2 and 4). The Western blot analysis above shows the relative amount of protein expressed in the whole cerebellar vermis, but not exclusively in PCs. However, the result of Western blotting combined with the electrophysiological data may imply that the *sg*/*sg* mutation would cause not only a decrease in mGluR1 expression in PCs, but also mislocalization of mGluR1, which might lead to the abolition of mGluR-mediated slow EPSCs in PCs. To test this possibility, we performed immunohistochemical analysis of mGluR1 in *staggerer* mutant cerebellum.

Figure 6 shows triple immunofluorescent staining of mGluR1, VGluT1 and calbindin in WT, +/*sg* and *sg*/*sg* mice. There was no difference in the distribution of mGluR1 between WT and +/*sg* cerebellum (Fig. 6*A* and *B*; left and middle rows). In these cerebella, immunofluorescence signals for mGluR1 were concentrated as a large number of tiny puncta along the dendrites of PCs (Fig. 6*B*, left and middle). These tiny puncta were scattered in the molecular layer (Fig. 6*A*, mGluR1, left and middle) and were closely associated or surrounded with VGluT1-labelled tiny puncta (putative presynaptic sites) (Fig. 6*B*, left and middle). On the other hand, in *sg*/*sg* mice, mGluR1-labelled signals were not scattered as tiny puncta, but were aggregated apparently randomly and frequently formed a continuous structure along the plasma membrane of PCs (Fig. 6*B*, right and 6*C*, right; white ovals indicate typical examples). Putative PF glutamate release sites (VGluT1-positive puncta) were much sparser

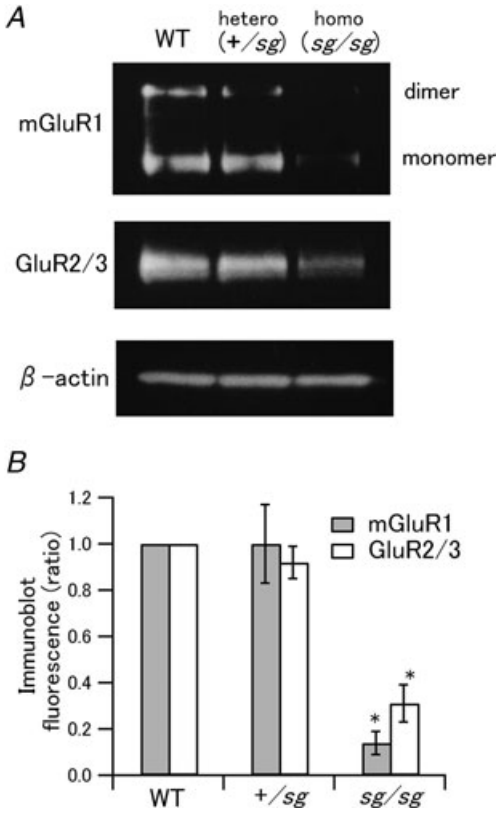

Figure 5. Expression levels of mGluR1 and GluR2/3 are reduced in *sg*/*sg* cerebellum
A, Western blot analysis showing expression levels of mGluR1 and GluR2/3 in WT, +/*sg* and *sg*/*sg* cerebella. Immunoblots of β-actin are shown as controls for the amount of total protein loading in each lane. *B*, quantified expression levels of mGluR1 (grey bars) and GluR2/3 (open bars) are normalized to the levels in WT mice (WT *versus* *sg*/*sg* and +/*sg* *versus* *sg*/*sg*, $^*P < 0.05$).

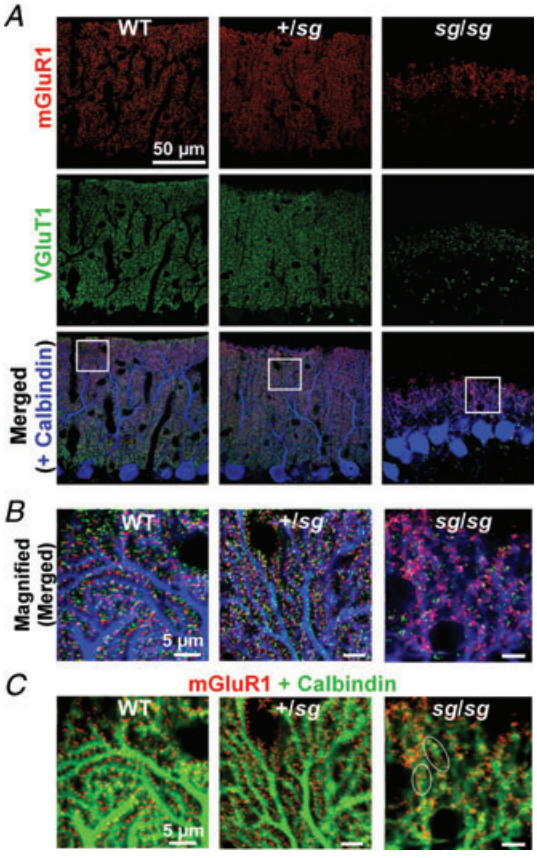

Figure 6. *Sg*/*sg* mutation causes mislocalization of mGluR1 on the dendrites of PCs
A and *B*, confocal images of cerebellar slices immunostained for mGluR1 (red), VGluT1 (green) and Calbindin (blue). Left, middle and right rows correspond to the images from WT, +/*sg* and *sg*/*sg* mice, respectively. The regions marked by white squares in *A* are enlarged in *B*. Scale bars represent 5 μm in *B*. *C*, the same images as in *B* except the images from two channels (mGluR1 and Calbindin) are superimposed and colour code for Calbindin (green) is different for a better view. White ovals indicate typical examples of continuous mGluR-positive signals along the plasma membrane of *sg*/*sg* PC. Scale bars represent 5 μm.

© 2011 The Authors. Journal compilation © 2011 The Physiological Society

(Fig. 6*A*, VGluT1, right) and spatially dispersed as in Fig. 3, and they did not surround the mGluR1-positive signals as in WT or in +/*sg* mice (Fig. 6*B*, right). These results suggest that most mGluR1s in *sg*/*sg* PCs may be located away from the release sites and mislocalized to non-synaptic or extrasynaptic sites. It has been shown that mGluR1 activation in PCs requires pooling of the released glutamate caused by simultaneous activation of adjacent PF synapses (synaptic cross talk between PF synapses) (Marcaggi & Attwell, 2005, 2007). Therefore, combined with our anatomical results above, lack of mGluR-mediated slow EPSCs in *sg*/*sg* mice could be ascribed to postsynaptic and presynaptic factors, that is an inappropriate amount and aberrant localization of mGluR1, and spatially dispersed presynaptic site, which would prevent synaptically released glutamate from accumulating enough to activate mislocalized mGluRs on *sg*/*sg* PCs.

Lack of DHPG-induced current and no expression of TRPC3 in *staggerer* PCs

The result of Fig. 4 demonstrates that *sg*/*sg* mice lack mGluR-mediated slow EPSCs at PF–PC synapses. This may be explained by the insufficient glutamate concentration experienced by mGluRs on *sg*/*sg* PCs due to mislocalization of mGluRs and/or sparse distribution of presynaptic release sites on PC dendrites (Fig. 6), as proposed in the previous section. Moreover, mGluR signalling itself could be dysfunctional in *sg*/*sg* PCs. To examine the functionality of all the mGluRs, including extrasynaptic mGluRs, without interference of presynaptic changes in *sg*/*sg* PCs, we bath-applied the mGluR1 agonist DHPG (100–200 μM) and monitored current responses from voltage-clamped PCs. In WT and +/*sg* mice, exogenous DHPG induced the inward current, which was apparently desensitized afterward (Fig. 7*A*, top and middle). In some cases, the DHPG-induced inward current was followed by a small, but discernable transient outward current (Fig. 7*A*, top). Desensitization and the outward current component of mGluR1-mediated currents have also been reported in other studies (Staub *et al.* 1992; Vranesic *et al.* 1993; Yamakawa & Hirano, 1999; Canepari *et al.* 2004; Becker *et al.* 2009). Although peak amplitudes of the DHPG-induced inward currents were variable (Fig. 7*B*, circles and triangles), DHPG always elicited the clearly resolved inward currents more than 150 pA in WT and +/*sg* PCs. On average, the peak amplitude was -826 ± 225 pA in WT ($n = 10$, 5 mice) and -1321 ± 156 pA in +/*sg* mice ($n = 9$, 3 mice). In contrast, *sg*/*sg* PCs had little, if any, DHPG-induced currents (Fig. 7*A*, bottom and 7*B*). The averaged peak amplitude was -49 ± 10 pA (Fig. 7*B*; $n = 10$, 3 *sg*/*sg* mice; Kruskal–Wallis test, $P < 0.001$; WT *versus* *sg*/*sg*, $P < 0.001$; +/*sg* *versus* *sg*/*sg*, $P < 0.001$; WT *versus* *sg*/*sg*, $P = 0.31$), which was comparable to the amplitude of the basal membrane current fluctuation (Fig. 7*A*, bottom) possibly caused by the intrinsic membrane properties of PCs and summated spontaneous synaptic inputs. On the other hand, bath application of 10 μM *RS*-AMPA, an AMPA receptor-specific agonist, induced robust inward currents more than 2.5 nA in all the recorded *sg*/*sg* PCs (Supplemental Fig. S1). Thus, we can rule out dysfunction of our perfusion system. Rather, the above results indicate that all the mGluRs in *sg*/*sg* PCs are dysfunctional and unable to produce slow excitatory inward currents.

Recently, it has been shown that the canonical transient receptor potential type 3 (TRPC3) channels underlie the generation of mGluR1-mediated slow currents in PCs (Hartmann *et al.* 2008). It is likely that the lack of mGluR-mediated slow inward currents in *sg*/*sg* PCs may also be ascribed to the abnormality of TRPC3 channels. To examine this hypothesis, we performed Western blot analysis of TRPC3 expressed in WT and mutant mice in the same way as in the previous section (Fig. 7*C*). The expression level of TRPC3 in +/*sg* cerebella was comparable to that in WT (0.98 ± 0.07 of WT, 5 mice). However, in *sg*/*sg* cerebella, the expression level was reduced significantly (0.17 ± 0.05 of WT, 5 mice; Kruskal–Wallis test, $P < 0.01$; WT *versus* *sg*/*sg*, $P < 0.05$; +/*sg* *versus* *sg*/*sg*, $P < 0.05$). Next, in order to examine the presence of TRPC3 subunits in PCs, we performed dual immunohistochemical staining for TRPC3 and calbindin in the cerebellar slice (Fig. 7*D*). In WT and +/*sg*, TRPC3 signals were distributed intensively in the molecular layer and the PC layer, and weakly in the granule cell layer (Fig. 7*D*, top and middle, magenta). Immunofluorescence for Calbindin (Fig. 7*D*, top and middle, green), which corresponded to PC structures, overlapped the TRPC3 immunofluorescence signals (Fig. 7*D*, top and middle, white), indicating that TRPC3 proteins are present in WT PCs and +/*sg* PCs as reported previously (Huang *et al.* 2007; Hartmann *et al.* 2008). In *sg*/*sg* cerebellum, although faint TRPC3 signals were observed, they had no overlap with PC morphology revealed by Calbindin immunofluorescence (Fig. 7*D*, bottom). Collectively, these results suggest that PCs in *sg*/*sg* mice have no TRPC3 subunits, leading to the abolition of mGluR1-mediated slow excitatory currents.

Disruption of mGluR1-mediated endocannabinoid-dependent retrograde suppression of AMPA-receptor-mediated EPSCs in *staggerer* PCs

It has been demonstrated that synaptic activation of mGluR1 in PCs induces local release of endogenous cannabinoid (endocannabinoid), which in turn acts

© 2011 The Authors. Journal compilation © 2011 The Physiological Society

on presynaptic type 1 cannabinoid (CB1) receptors and thereby suppresses glutamate release from PFs retrogradely for a short time (tens of seconds) (Safo *et al.* 2006; Hashimotodani *et al.* 2007; Ferraguti *et al.* 2008; Kano *et al.* 2008, 2009; Best & Regehr, 2010). Therefore, impairment of mGluR signalling in PCs would affect this endocannabinoid-mediated short-term plasticity at PF–PC synapses. To elucidate the functional consequences of mGluR signalling deficiency in *sg*/*sg* mice, we examined the above-mentioned endocannabinoid-mediated changes in synaptic strength, which is termed synaptically evoked suppression of excitation (SSE).

After monitoring basal PF-evoked EPSCs in PCs, we applied a burst of high frequency PF stimulation (PF burst, a train of 50 stimuli at 100 Hz) to activate mGluRs enough to elicit SSE (Brown *et al.* 2003; Marcaggi & Attwell, 2005; Tanimura *et al.* 2010). PF bursts reliably led to SSE, that is a decrease in the subsequent PF-evoked EPSCs in WT (Fig. 8*A*, top and 8*B*, open circles) and +/*sg* mice (Fig. 8*A*, middle and 8*B*, grey filled circles; normalized amplitude of the first EPSC after PF burst to the mean basal EPSCs: WT, 0.42 ± 0.06, $n = 6$, 4 mice; +/*sg*, 0.53 ± 0.05, $n = 7$, 3 mice). In WT, bath application of the CB1 receptor antagonist AM251 (5 μM) eliminated SSE and unveiled a transient potentiation (Fig. 8*A*, top, inset and 8B, triangles), which is generally categorized as post-tetanic potentiation (PTP) (Zucker & Regehr, 2002) and is caused by Ca^{2+} elevations in presynaptic PF terminals followed by activation of protein kinase C (Beierlein *et al.* 2007). This observation is consistent with previous studies (Beierlein *et al.* 2007; Marcaggi & Attwell, 2007; Tanimura *et al.* 2010) and confirms that PF burst-induced SSE in this study is caused by endocannabinoid release and consequent activation of CB1 receptors. In *sg*/*sg* PCs, SSE was absent, and instead the PF

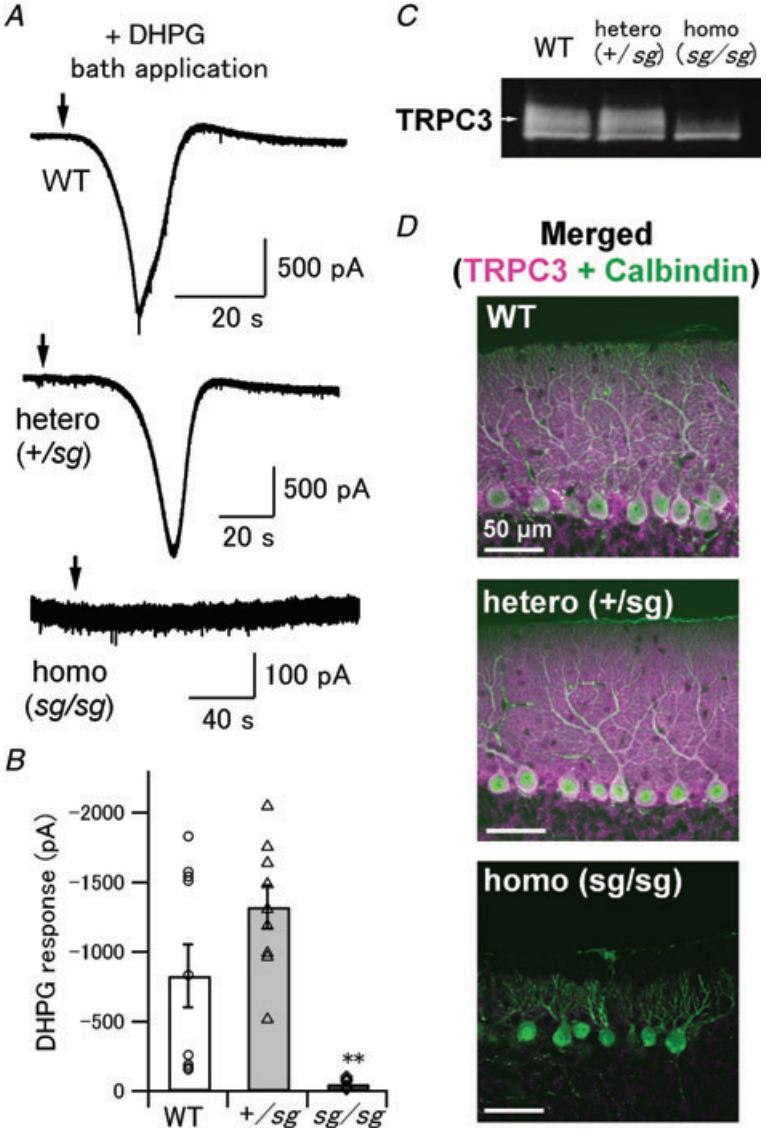

Figure 7. No DHPG-induced current and low expression levels of TRPC3 in *sg*/*sg* PCs
A, an mGluR1 agonist, DHPG (100–200 μM), was bath-applied to activate all the mGluRs on PCs. Each arrow indicates the time point when the DHPG solution reached the recording chamber. *B*, pooled data of DHPG-induced responses in WT, +/*sg* and *sg*/*sg* PCs. Symbols and bar graphs correspond to individual data points and mean values of the peak amplitudes, respectively (WT *versus* *sg*/*sg* and +/*sg* *versus* *sg*/*sg*, $^{**}P < 0.001$). *C*, immunoblots showing expression levels of TRPC3 in WT, +/*sg* and *sg*/*sg* cerebella. A white arrow indicates the expected MW of TRPC3 (~100 kDa). *D*, confocal images of the cerebellar slices double-immunostained for TRPC3 (magenta) and Calbindin (green). White signals indicate colocalization of TRPC3 with Calbindin, which means that TRPC3 proteins are present in PCs. Scale bars represent 50 μm.

© 2011 The Authors. Journal compilation © 2011 The Physiological Society

burst induced PTP, which resembles the WT phenotype in the presence of AM251 (Fig. 8*A*, bottom and 8*B*, black filled circles), although the degree of potentiation was smaller than that in WT and the smaller PTP might be ascribed to increased initial release probability at PF–PC synapses in *sg*/*sg* mice (Beierlein *et al.* 2007). These results could be ascribed to impairment of mGluR signalling in *sg*/*sg* PCs.

However, apart from the mGluR signalling pathway, *sg*/*sg* mice might have some defects in the endocannabinoid-mediated signalling pathway itself including endocannabinoid release from PCs and activation of presynaptic CB1 receptors. To test this possibility, we examined the mGluR-independent form of endocannabinoid-mediated retrograde signalling, depolarization-induced suppression of excitation (DSE). For DSE, endocannabinoid release from PCs is driven solely by an exceptionally large increase in intracellular calcium (in the range of a few micromolar), which is induced by depolarization, and does not rely on the activation of mGluRs (Safo *et al.* 2006; Hashimotodani *et al.* 2007; Kano *et al.* 2009; Best & Regehr, 2010). In WT, after PCs were depolarized from −70 mV to 0 mV for 5 s (Tanimura *et al.* 2010), subsequent first PF-evoked EPSCs were reduced to 0.69 ± 0.02 ($n = 10$) of the mean basal EPSCs measured before depolarization (Fig. 8*C*, top and 8*D*, open circles). Application of AM251 (5 μM) blocked the DSE (Fig. 8*C*, top, inset). Both in +/*sg* and in *sg*/*sg* PCs, DSE was clearly observed to the same degree (normalized amplitude of 1st EPSC after depolarization: +/*sg*, 0.54 ± 0.07, $n = 5$, 4 mice; *sg*/*sg*, 0.53 ± 0.05, $n = 3$, 3 mice) (Fig. 8*C*, middle and 8*C*, bottom), although the degree of suppression in *staggerer* mutant mice was slightly larger than in WT (Fig. 8*D*). These results indicate that *sg*/*sg* PCs have intact endocannabinoid-mediated retrograde signalling, that is, undisturbed endocannabinoid-producing capacity and presynaptic CB1-receptor function. Therefore, we conclude that impairment of mGluR1 signalling in *sg*/*sg* mice leads to malfunction of synaptically evoked mGluR1-mediated endocannabinoid retrograde modulation at PF–PC synapses.

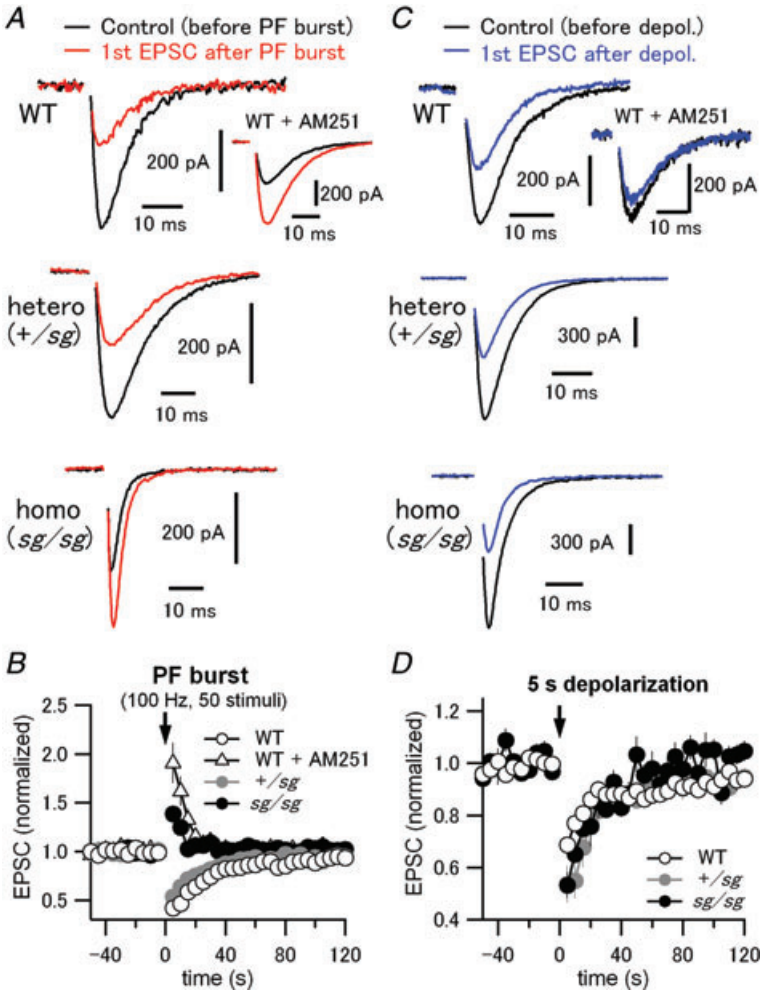

Figure 8. Disruption of mGluR signalling abolishes synaptically induced endocannabinoid-mediated retrograde suppression of PF EPSCs in *sg*/*sg* PCs
A, PF-evoked EPSCs were monitored in PCs every 5 s. After recording 10 stable basal EPSCs, a high frequency PF stimulus train (PF burst, 50 pulses at 100 Hz) was applied to activate an mGluR-mediated signalling cascade which causes endocannabinoid-dependent retrograde suppression of PF EPSCs for tens of seconds. After PF burst, 24 PF EPSCs were recorded to monitor such short-term plasticity, which is also known as synaptically evoked suppression of excitation (SSE). Black and red traces represent the last EPSC of the basal EPSC recordings (the EPSC just before PF burst) and the first EPSC after PF burst in each experimental condition, respectively. Inset in the top panel shows the traces obtained in the same way except from a different PC in the presence of a CB1-receptor antagonist, AM251 (5 μM). *B*, peak amplitudes of all the recorded EPSCs were normalized to averaged peak amplitudes of 6 basal EPSCs evoked before PF burst. Each data point represents mean normalized amplitude plotted against the recording time. An arrow indicates the time point zero when the PF burst was applied. *C* and *D*, depolarization-induced suppression of excitation (DSE), where endocannabinoid release from PCs depends solely on a large intracellular Ca^{2+} increase, but not on activation of mGluRs. Experimental protocol and data analysis were the same as in *A* and *B*, except that a 5 s depolarizing pulse to 0 mV was applied to PCs instead of PF burst for induction of DSE. In contrast to the SSE data in *A* and *B*, DSE was reliably observed in WT and *staggerer* mutant mice, indicating that endocannabinoid production and presynaptic CB1-receptor function are both intact in the mutants.

© 2011 The Authors. Journal compilation © 2011 The Physiological Society

Discussion

It has been suggested that cerebellar PCs in *staggerer* mutant mice are developmentally retarded and morphologically aberrant: however, the functional properties of immature junctions formed between PFs and PCs have remained unclear. In the present study, we have shown that PCs in *sg*/*sg* mice establish some of functional glutamatergic PF–PC synapses (Figs 2 and 3), which exhibit slightly attenuated PPF at short intervals (Fig. 2) and faster EPSC kinetics (Fig. 2) that could be attributed to the morphological abnormalities of PCs (Fig. 1). Surprisingly, in *sg*/*sg* mice, mGluR1-mediated slow currents were not induced by intense PF burst stimulation (Fig. 4), nor exogenous mGluR1 agonist, DHPG (Fig. 7). This is most likely caused by the greatly reduced expression of mGluR1 and TRPC3 in *sg*/*sg* cerebella (Figs 5 and 7), mislocalization of mGluR1 (Fig. 6) and absence of TRPC3 in *sg*/*sg* PCs (Fig. 7). The influence of disrupted mGluR signalling in *sg*/*sg* mice is not limited to mGluR-mediated slow currents, but results in a defect in mGluR-mediated retrograde suppression of PF EPSCs via endocannabinoid release, in spite of the intact depolarization-induced release of endocannabinoid and subsequent retrograde suppression of PF EPSCs (Fig. 8).

Altered short-term plasticity at PF–PC synapses in *sg*/*sg* mice

Homeostatic synaptic plasticity occurs in order to maintain postsynaptic excitability in an appropriate range by adjusting the synaptic strength (Rich & Wenner, 2007; Regehr *et al.* 2009; Yu & Goda, 2009). Such homeostatic plasticity should also occur in *sg*/*sg* PCs. Since synaptic inputs from PFs are reduced in *sg*/*sg* mice due to far fewer PF–PC synapses, the initial release probability at each synapse might be increased to compensate for the reduced synaptic inputs, resulting in decreased PPF (Dobrunz & Stevens, 1997) at *sg*/*sg* PF–PC synapses.

Various postsynaptic molecules could affect short-term plasticity including PPF retrogradely in a homeostatic way (Yu & Goda, 2009). Reduced PPF at *sg*/*sg* PF–PC synapses cannot be ascribed to the reduced expression of GluRδ2 (data not shown) since GluRδ2-deficient mice show increased PPF (Kashiwabuchi *et al.* 1995; Kakegawa *et al.* 2008). Lack of mGluR1 signalling in *sg*/*sg* PCs might explain the decreased PPF, because PPF at PF–PC synapses tends to be smaller in mGluR1-lacking mice than in WT although there is not a statistically significant difference (Aiba *et al.* 1994). It should be mentioned that gene disruption of brain-derived neurotrophic factor (Carter *et al.* 2002) or Ca^{2+}-dependent activator protein for secretion 2 (CAPS2) (Sadakata *et al.* 2007) decreases PPF at PF–PC synapses for brief intervals, similar to the *sg*/*sg* phenotype. Brain-derived neurotrophic factor and CAPS2 are abundant in PF synaptic boutons and CAPS2 is involved in the release of brain-derived neurotrophic factor and neurotrophin-3 (Sadakata & Furuichi, 2009). Interestingly, these molecules are also required for normal cerebellar development (Sadakata & Furuichi, 2009) and mRNA levels of brain-derived neurotrophic factor and neurotrophin-3 in the internal granular layer are reduced in *sg*/*sg* cerebellum (Qiu *et al.* 2007). These molecules might be involved in altered PPF in *sg*/*sg* mice under direct or indirect control of RORα. Moreover, PPF is determined by volume-averaged global Ca^{2+} signal (residual Ca^{2+}) in PF terminals (Atluri & Regehr, 1996). The *sg*/*sg* mutation might alter residual Ca^{2+} signals in PF terminals.

Contribution of mGluR1 defect to the ataxic phenotype in *sg*/*sg* mice

The mGluR1 is highly expressed in PCs, in which the protein is localized at the perisynaptic regions of Purkinje cell dendrites facing PF synaptic terminals (Baude *et al.* 1993; Nusser *et al.* 1994). The mGluR1 knock-out mouse exhibits prominent ataxia without any alteration in cerebellar morphology and basic properties of excitatory synaptic transmission (Aiba *et al.* 1994), and PC-specific genetic rescue of the mGluR1 expression reliably restores the ataxia of mutant mice (Ichise *et al.* 2000). Moreover, autoantibodies against mGluR1 protein cause cerebellar ataxia in adult patients with Hodgkin's disease, and wild-type mice that receive anti-mGluR1 antibodies from those patients also exhibit cerebellar ataxia (Sillevis Smitt *et al.* 2000; Coesmans *et al.* 2003). These findings strongly suggest that mGluR1 in PCs plays critical roles in motor coordination, and that impairment of mGluR1 results in cerebellar ataxia. Thus, markedly reduced expression levels and mislocalization of mGluR1 protein (Figs 5 and 6), and disruption of mGluR1 signalling in staggerer PCs (Figs 4 and 7) revealed in the present study, could underlie the ataxic phenotype of *staggerer* mice.

In PCs, mGluR1 is coupled to mainly Gq protein and, to a lesser extent, G_{11} (Hartmann *et al.* 2004). Activation of both G proteins via mGluR1 stimulates phospholipase Cβ, which cleaves phosphatidylinositol bisphosphate into diacylglycerol and inositol trisphosphate (IP_3) (Hashimotodani *et al.* 2007; Ferraguti *et al.* 2008; Hartmann & Konnerth, 2009). Through these enzymatic reactions, mGluR1 triggers four distinct cellular events: (1) cation influx by opening of TRPC3 channels, producing slow EPSC in PCs (Tempia *et al.* 1998; Canepari *et al.* 2001; Hartmann *et al.* 2008), (2) Ca^{2+} release from the endoplasmic reticulum upon IP_3 binding to IP_3 receptors, causing mGluR-mediated transient Ca^{2+} signalling (Finch & Augustine, 1998; Takechi *et al.* 1998; Hartmann *et al.* 2008), (3) diacylglycerol-dependent activation of protein kinase C, an enzyme critical for long-term depression at

© 2011 The Authors. Journal compilation © 2011 The Physiological Society

PF–PC synapses (Kano *et al.* 2008), and (4) diacylglycerol lipase α-mediated conversion of diacylglycerol into endocannabinoids, which retrogradely activate presynaptic CB1 receptors, leading to the suppression of presynaptic transmitter release (Best & Regehr, 2010; Tanimura *et al.* 2010). Since mice lacking TRPC3 channels (Hartmann *et al.* 2008) or IP_3 receptors (Matsumoto *et al.* 1996) are apparently ataxic, defects in those downstream signalling cascades of mGluR could be more directly involved in motor discoordination in *staggerer* mice as well as mGluR1-deficient mice. Interestingly, abnormal enhancement of TRPC3 channels is also reported to be involved in cerebellar ataxia in moonwalker mutant mice (Becker *et al.* 2009).

Endocannabinoid signalling pathways

The present study shows that mGluR-mediated endocannabinoid release (i.e. SSE) is abolished while depolarization-induced endocannabinoid release (i.e. DSE) is intact in *sg*/*sg* PCs. This is in line with the case of phospholipase Cβ-deficient mice, in which the downstream cascade of mGluR signalling is disturbed and the component of mGluR-independent DSE (Ca^{2+}-driven endocannabinoid release) is not affected (Maejima *et al.* 2005). These findings support two separate pathways of endocannabinoid production (Hashimotodani *et al.* 2007; Best & Regehr, 2010). Interestingly, diacylglycerol lipase α-lacking mice exhibit disruption of both SSE and DSE (Tanimura *et al.* 2010). This indicates that the two separate cascades of endocannabinoid production in PCs converge before its release (Hashimotodani *et al.* 2007; Best & Regehr, 2010). The exact molecular pathway during DSE remains to be identified.

Potential impact of the *sg*/*sg* mutation beyond cerebellum

RORα is widely expressed in neuronal and non-neuronal tissues such as olfactory bulb, hypothalamus, thalamus, retina, thymus, skin, testis and so on (Boukhtouche *et al.* 2006). Some of them (e.g. mitral cells of the olfactory bulb, suprachiasmatic nucleus, retinal amacrine and ganglion cells, thalamic relay nuclei and some thymocytes) also express mGluR1 (Tehrani *et al.* 2000; Ferraguti & Shigemoto, 2006; Nicoletti *et al.* 2007; Ferraguti *et al.* 2008) and thus the *sg*/*sg* mutation of RORα may cause mGluR-related functional defects on those neuronal and immune tissues. In mitral cells of the olfactory bulb, mGluR1 is involved in slow potentials, oscillations, Ca^{2+} signalling and regulation of excitability (Yuan & Knopfel, 2006; Heinbockel *et al.* 2007). In fact, odour-induced evoked field potentials in the mitral cell layer are reduced and the olfactory bulb is structurally disorganized in *sg*/*sg* mice (Monnier *et al.* 1999; Michel *et al.* 2000). Interestingly, in the hypothalamic suprachiasmatic nucleus, not only RORα (Boukhtouche *et al.* 2006) but also group I mGluR (Park *et al.* 2003) has been shown to play a role in circadian rhythms. In retinal amacrine and ganglion cells, mGluR1 is shown to mediate long-term plasticity of GABAergic feedback inhibition at reciprocal synapses (Vigh *et al.* 2005) and modulation of intrinsic excitability (Yu *et al.* 2009), respectively. In thalamic relay neurons, activation of mGluR1 causes an intrinsic slow (<1 Hz) oscillation, leading to generation of the slow sleep rhythm (Hughes *et al.* 2002). The thalamic mGluR1-phospholipase Cβ4 cascade is suggested to be essential for inflammatory pain processing (Miyata *et al.* 2003). It would be interesting to see whether these mGluR functions are affected in *sg*/*sg* mice.

Implication of the *sg*/*sg* mutation in SCA1 pathology

The *sg*/*sg* mutation is suggested to be closely related to SCA1, a neurodegenerative disorder caused by abnormal CAG repeat expansion in ataxin-1, since ataxin-1 forms a transcriptional complex with RORα via the transcriptional coactivator Tip60 (Serra *et al.* 2006). The complex binds to a set of promoters and initiates the transactivation of RORα target genes (Gold *et al.* 2003). In SCA1 model mice, the transcriptional complex containing ataxin-1, Tip60 and RORα may not be formed properly because conformational change in the mutant ataxin-1 might induce the destabilization of RORα, and eventually, free RORα may be degraded, resulting in the disruption of RORα-regulated gene expression (Serra *et al.* 2006) as in the case of *staggerer* mice carrying loss-of-function mutant RORα (Boukhtouche *et al.* 2006; Gold *et al.* 2007). Interestingly, mGluR1 is one of the genes which decreases in expression both in SCA1 mice and *sg*/*sg* mice. Moreover, mGluR1 expression is critical for the recovery of SCA1 mice from ataxia: in conditional SCA1 mice that express mutant ataxin-1 under the tetracycline-controlled (tet-off) system, motor discoordination continues even after removal of mutant ataxin-1 itself from PCs and motor recovery is in parallel with the re-expression of mGluR1 protein at PF–PC synapses (Zu *et al.* 2004). Therefore, mGluR1 is thought to be a key molecule in the pathogenesis of SCA1. The present study provides the first electrophysiological evidence that mGluR1 signalling is completely disrupted in *sg*/*sg* PCs, despite the formation of functional PF–PC synapses. Although RORα regulates the expression of various proteins, disruption of mGluR1 signalling would be a major direct cause of ataxic phenotypes in *sg*/*sg* mice. Expression of Homer-3, an adaptor protein of mGluR1, is decreased in *sg*/*sg* mice (data not shown) and SCA1 mice (Serra *et al.* 2004), which might underlie the mislocalization and/or

© 2011 The Authors. Journal compilation © 2011 The Physiological Society

dysfunction of mGluR1 in *sg*/*sg* mice. It should be noted that although *sg*/*sg* mice have defects in cerebellar development, disruption of the mGluR1 pathway after complete maturation of the cerebellum still causes ataxia in adult mice (Sillevis Smitt *et al.* 2000; Nakao *et al.* 2007), indicating that mGluR1 signalling is essential for proper cerebellar function in adulthood. In SCA1 model mice, the expression of TRPC3 is also downregulated (Lin *et al.* 2000), similar to our results in *sg*/*sg* mice (Fig. 7*C* and *D*). This may imply that TRPC3 is also one of the potential target genes of RORα. Rescue of mGluR signalling by gene transfer techniques might rescue or mitigate ataxia in SCA1 patients.

Both SCA1 and *sg*/*sg* mutations involve PC degeneration (Zu *et al.* 2004; Boukhtouche *et al.* 2006). However, mGluR1-deficient mice do not cause PC degeneration (Aiba *et al.* 1994; Kano *et al.* 1997), suggesting that other genes regulated by RORα may contribute to PC degeneration. In addition to mGluR1, the RORα-regulated gene set, especially the downregulated one in *sg*/*sg* and SCA1 mice, includes Slc1a6 (PC glutamate transporter, EAAT4), Spnb3 (brain-specific β-spectrin III which anchors EAAT4 to the cytoskeleton; mutations in Spnb3 lead to SCA5), Itpr1 (IP_3 receptor 1, mutation of which causes SCA15), Calb1 (calbindin D-28k, Ca^{2+} buffer protein), Pcp4 (calmodulin inhibitor), Pcp2/L7 (Goloco G protein modulatory domain, which is shown to modulate P/Q-type voltage-gated Ca^{2+} channels present in PCs; Kinoshita-Kawada *et al.* 2004), Cals1 (an IP_3 receptor 1 binding partner), and Atp2a2 (Ca^{2+}-transporting ATPase, also called SERCA2) (Gold *et al.* 2003; Serra *et al.* 2006). These RORα-regulated factors, most of which mediate Ca^{2+}-dependent signalling in PCs, might be involved in PC degeneration (Liu *et al.* 2009). The *sg*/*sg* mouse is a useful model for elucidating SCA1 pathogenesis as well as the physiological functions of RORα, and further work remains to be done to gain insight into underlying mechanisms of cerebellar pathology.

References

Aiba A, Kano M, Chen C, Stanton ME, Fox GD, Herrup K, Zwingman TA & Tonegawa S (1994). Deficient cerebellar long-term depression and impaired motor learning in mGluR1 mutant mice. *Cell* **79**, 377–388.

Atluri PP & Regehr WG (1996). Determinants of the time course of facilitation at the granule cell to Purkinje cell synapse. *J Neurosci* **16**, 5661–5671.

Bastianelli E (2003). Distribution of calcium-binding proteins in the cerebellum. *Cerebellum* **2**, 242–262.

Batchelor AM, Madge DJ & Garthwaite J (1994). Synaptic activation of metabotropic glutamate receptors in the parallel fibre-Purkinje cell pathway in rat cerebellar slices. *Neuroscience* **63**, 911–915.

Baude A, Nusser Z, Roberts JD, Mulvihill E, McIlhinney RA & Somogyi P (1993). The metabotropic glutamate receptor (mGluR1α) is concentrated at perisynaptic membrane of neuronal subpopulations as detected by immunogold reaction. *Neuron* **11**, 771–787.

Becker EB, Oliver PL, Glitsch MD, Banks GT, Achilli F, Hardy A, Nolan PM, Fisher EM & Davies KE (2009). A point mutation in TRPC3 causes abnormal Purkinje cell development and cerebellar ataxia in moonwalker mice. *Proc Natl Acad Sci U S A* **106**, 6706–6711.

Beierlein M, Fioravante D & Regehr WG (2007). Differential expression of posttetanic potentiation and retrograde signaling mediate target-dependent short-term synaptic plasticity. *Neuron* **54**, 949–959.

Bekkers JM & Hausser M (2007). Targeted dendrotomy reveals active and passive contributions of the dendritic tree to synaptic integration and neuronal output. *Proc Natl Acad Sci U S A* **104**, 11447–11452.

Berry M, Bradley P & Borges S (1978). Environmental and genetic determinants of connectivity in the central nervous system – an approach through dendritic field analysis. *Prog Brain Res* **48**, 133–148.

Best AR & Regehr WG (2010). Identification of the synthetic pathway producing the endocannabinoid that mediates the bulk of retrograde signaling in the brain. *Neuron* **65**, 291–292.

Boukhtouche F, Doulazmi M, Frederic F, Dusart I, Brugg B & Mariani J (2006). RORα, a pivotal nuclear receptor for Purkinje neuron survival and differentiation: from development to ageing. *Cerebellum* **5**, 97–104.

Bradley P & Berry M (1978). The Purkinje cell dendritic tree in mutant mouse cerebellum. A quantitative Golgi study of *Weaver* and *Staggerer* mice. *Brain Res* **142**, 135–141.

Brown SP, Brenowitz SD & Regehr WG (2003). Brief presynaptic bursts evoke synapse-specific retrograde inhibition mediated by endogenous cannabinoids. *Nat Neurosci* **6**, 1048–1057.

Burnashev N, Khodorova A, Jonas P, Helm PJ, Wisden W, Monyer H, Seeburg PH & Sakmann B (1992). Calcium-permeable AMPA-kainate receptors in fusiform cerebellar glial cells. *Science* **256**, 1566–1570.

Canepari M, Auger C & Ogden D (2004). Ca^{2+} ion permeability and single-channel properties of the metabotropic slow EPSC of rat Purkinje neurons. *J Neurosci* **24**, 3563–3573.

Canepari M, Papageorgiou G, Corrie JE, Watkins C & Ogden D (2001). The conductance underlying the parallel fibre slow EPSP in rat cerebellar Purkinje neurones studied with photolytic release of L-glutamate. *J Physiol* **533**, 765–772.

Carter AR, Chen C, Schwartz PM & Segal RA (2002). Brain-derived neurotrophic factor modulates cerebellar plasticity and synaptic ultrastructure. *J Neurosci* **22**, 1316–1327.

Coesmans M, Smitt PA, Linden DJ, Shigemoto R, Hirano T, Yamakawa Y, van Alphen AM, Luo C, Van Der Geest JN, Kros JM, Gaillard CA, Frens MA & de Zeeuw CI (2003). Mechanisms underlying cerebellar motor deficits due to mGluR1-autoantibodies. *Ann Neurol* **53**, 325–336.

© 2011 The Authors. Journal compilation © 2011 The Physiological Society

Crepel F, Delhaye-Bouchaud N, Guastavino JM & Sampaio I (1980). Multiple innervation of cerebellar Purkinje cells by climbing fibres in *staggerer* mutant mouse. *Nature* **283**, 483–484.

Crepel F, Dupont JL & Gardette R (1984). Selective absence of calcium spikes in Purkinje cells of *staggerer* mutant mice in cerebellar slices maintained in vitro. *J Physiol* **346**, 111–125.

Dobrunz LE & Stevens CF (1997). Heterogeneity of release probability, facilitation, and depletion at central synapses. *Neuron* **18**, 995–1008.

Doulazmi M, Frederic F, Capone F, Becker-Andre M, Delhaye-Bouchaud N & Mariani J (2001). A comparative study of Purkinje cells in two RORα gene mutant mice: staggerer and RORα(–/–). *Brain Res Dev Brain Res* **127**, 165–174.

Drummond GB (2009). Reporting ethical matters in *The Journal of Physiology*: standards and advice. *J Physiol* **587**, 713–719.

Ferraguti F, Crepaldi L & Nicoletti F (2008). Metabotropic glutamate 1 receptor: current concepts and perspectives. *Pharmacol Rev* **60**, 536–581.

Ferraguti F & Shigemoto R (2006). Metabotropic glutamate receptors. *Cell Tissue Res* **326**, 483–504.

Finch EA & Augustine GJ (1998). Local calcium signalling by inositol-1,4,5-trisphosphate in Purkinje cell dendrites. *Nature* **396**, 753–756.

Fremeau RT Jr, Troyer MD, Pahner I, Nygaard GO, Tran CH, Reimer RJ, Bellocchio EE, Fortin D, Storm-Mathisen J & Edwards RH (2001). The expression of vesicular glutamate transporters defines two classes of excitatory synapse. *Neuron* **31**, 247–260.

Gold DA, Baek SH, Schork NJ, Rose DW, Larsen DD, Sachs BD, Rosenfeld MG & Hamilton BA (2003). RORalpha coordinates reciprocal signaling in cerebellar development through sonic hedgehog and calcium-dependent pathways. *Neuron* **40**, 1119–1131.

Gold DA, Gent PM & Hamilton BA (2007). RORα in genetic control of cerebellum development: 50 staggering years. *Brain Res* **1140**, 19–25.

Hamilton BA, Frankel WN, Kerrebrock AW, Hawkins TL, FitzHugh W, Kusumi K, Russell LB, Mueller KL, van Berkel V, Birren BW, Kruglyak L & Lander ES (1996). Disruption of the nuclear hormone receptor RORα in *staggerer* mice. *Nature* **379**, 736–739.

Hartmann J, Blum R, Kovalchuk Y, Adelsberger H, Kuner R, Durand GM, Miyata M, Kano M, Offermanns S & Konnerth A (2004). Distinct roles of $G\alpha_q$ and $G\alpha_{11}$ for Purkinje cell signaling and motor behavior. *J Neurosci* **24**, 5119–5130.

Hartmann J, Dragicevic E, Adelsberger H, Henning HA, Sumser M, Abramowitz J, Blum R, Dietrich A, Freichel M, Flockerzi V, Birnbaumer L & Konnerth A (2008). TRPC3 channels are required for synaptic transmission and motor coordination. *Neuron* **59**, 392–398.

Hartmann J & Konnerth A (2009). Mechanisms of metabotropic glutamate receptor-mediated synaptic signaling in cerebellar Purkinje cells. *Acta Physiol (Oxf)* **195**, 79–90.

Hashimotodani Y, Ohno-Shosaku T & Kano M (2007). Ca^{2+}-assisted receptor-driven endocannabinoid release: mechanisms that associate presynaptic and postsynaptic activities. *Curr Opin Neurobiol* **17**, 360–365.

Heinbockel T, Laaris N & Ennis M (2007). Metabotropic glutamate receptors in the main olfactory bulb drive granule cell-mediated inhibition. *J Neurophysiol* **97**, 858–870.

Herrup K & Mullen RJ (1981). Role of the Staggerer gene in determining Purkinje cell number in the cerebellar cortex of mouse chimeras. *Brain Res* **227**, 475–485.

Hirai H, Launey T, Mikawa S, Torashima T, Yanagihara D, Kasaura T, Miyamoto A & Yuzaki M (2003). New role of delta2-glutamate receptors in AMPA receptor trafficking and cerebellar function. *Nat Neurosci* **6**, 869–876.

Hirano A & Dembitzer HM (1975). The fine structure of *staggerer* cerebellum. *J Neuropathol Exp Neurol* **34**, 1–11.

Huang WC, Young JS & Glitsch MD (2007). Changes in TRPC channel expression during postnatal development of cerebellar neurons. *Cell Calcium* **42**, 1–10.

Hughes SW, Cope DW, Blethyn KL & Crunelli V (2002). Cellular mechanisms of the slow ($<$1 Hz) oscillation in thalamocortical neurons in vitro. *Neuron* **33**, 947–958.

Ichise T, Kano M, Hashimoto K, Yanagihara D, Nakao K, Shigemoto R, Katsuki M & Aiba A (2000). mGluR1 in cerebellar Purkinje cells essential for long-term depression, synapse elimination, and motor coordination. *Science* **288**, 1832–1835.

Ino H (2004). Immunohistochemical characterization of the orphan nuclear receptor RORα in the mouse nervous system. *J Histochem Cytochem* **52**, 311–323.

Janmaat S, Frederic F, Sjollema K, Luiten P, Mariani J & Van Der Want J (2009). Formation and maturation of parallel fiber-Purkinje cell synapses in the *Staggerer* cerebellum ex vivo. *J Comp Neurol* **512**, 467–477.

Kakegawa W, Miyazaki T, Emi K, Matsuda K, Kohda K, Motohashi J, Mishina M, Kawahara S, Watanabe M & Yuzaki M (2008). Differential regulation of synaptic plasticity and cerebellar motor learning by the C-terminal PDZ-binding motif of GluRδ2. *J Neurosci* **28**, 1460–1468.

Kano M, Hashimoto K, Kurihara H, Watanabe M, Inoue Y, Aiba A & Tonegawa S (1997). Persistent multiple climbing fiber innervation of cerebellar Purkinje cells in mice lacking mGluR1. *Neuron* **18**, 71–79.

Kano M, Hashimoto K & Tabata T (2008). Type-1 metabotropic glutamate receptor in cerebellar Purkinje cells: a key molecule responsible for long-term depression, endocannabinoid signalling and synapse elimination. *Philos Trans R Soc Lond B Biol Sci* **363**, 2173–2186.

Kano M, Ohno-Shosaku T, Hashimotodani Y, Uchigashima M & Watanabe M (2009). Endocannabinoid-mediated control of synaptic transmission. *Physiol Rev* **89**, 309–380.

Kashiwabuchi N, Ikeda K, Araki K, Hirano T, Shibuki K, Takayama C, Inoue Y, Kutsuwada T, Yagi T, Kang Y, *et al.* (1995). Impairment of motor coordination, Purkinje cell synapse formation, and cerebellar long-term depression in GluRδ2 mutant mice. *Cell* **81**, 245–252.

Kinoshita-Kawada M, Oberdick J & Xi Zhu M (2004). A Purkinje cell specific GoLoco domain protein, L7/Pcp-2, modulates receptor-mediated inhibition of Cav2.1 Ca^{2+} channels in a dose-dependent manner. *Brain Res Mol Brain Res* **132**, 73–86.

Knopfel T & Grandes P (2002). Metabotropic glutamate receptors in the cerebellum with a focus on their function in Purkinje cells. *Cerebellum* **1**, 19–26.

© 2011 The Authors. Journal compilation © 2011 The Physiological Society

Konnerth A, Llano I & Armstrong CM (1990). Synaptic currents in cerebellar Purkinje cells. *Proc Natl Acad Sci U S A* **87**, 2662–2665.

Landis DM & Reese TS (1977). Structure of the Purkinje cell membrane in *staggerer* and *weaver* mutant mice. *J Comp Neurol* **171**, 247–260.

Landis DM & Sidman RL (1978). Electron microscopic analysis of postnatal histogenesis in the cerebellar cortex of *staggerer* mutant mice. *J Comp Neurol* **179**, 831–863.

Lin X, Antalffy B, Kang D, Orr HT & Zoghbi HY (2000). Polyglutamine expansion down-regulates specific neuronal genes before pathologic changes in SCA1. *Nat Neurosci* **3**, 157–163.

Liu J, Tang TS, Tu H, Nelson O, Herndon E, Huynh DP, Pulst SM & Bezprozvanny I (2009). Deranged calcium signaling and neurodegeneration in spinocerebellar ataxia type 2. *J Neurosci* **29**, 9148–9162.

Llano I, Marty A, Armstrong CM & Konnerth A (1991). Synaptic- and agonist-induced excitatory currents of Purkinje cells in rat cerebellar slices. *J Physiol* **434**, 183–213.

Maejima T, Oka S, Hashimotodani Y, Ohno-Shosaku T, Aiba A, Wu D, Waku K, Sugiura T & Kano M (2005). Synaptically driven endocannabinoid release requires Ca^{2+}-assisted metabotropic glutamate receptor subtype 1 to phospholipase Cβ4 signaling cascade in the cerebellum. *J Neurosci* **25**, 6826–6835.

Marcaggi P & Attwell D (2005). Endocannabinoid signaling depends on the spatial pattern of synapse activation. *Nat Neurosci* **8**, 776–781.

Marcaggi P & Attwell D (2007). Short- and long-term depression of rat cerebellar parallel fibre synaptic transmission mediated by synaptic crosstalk. *J Physiol* **578**, 545–550.

Mariani J & Changeux JP (1980). Multiple innervation of Purkinje cells by climbing fibers in the cerebellum of the adult staggerer mutant mouse. *J Neurobiol* **11**, 41–50.

Matsuda S, Mikawa S & Hirai H (1999). Phosphorylation of serine-880 in GluR2 by protein kinase C prevents its C terminus from binding with glutamate receptor-interacting protein. *J Neurochem* **73**, 1765–1768.

Matsumoto M, Nakagawa T, Inoue T, Nagata E, Tanaka K, Takano H, Minowa O, Kuno J, Sakakibara S, Yamada M, Yoneshima H, Miyawaki A, Fukuuchi Y, Furuichi T, Okano H, Mikoshiba K & Noda T (1996). Ataxia and epileptic seizures in mice lacking type 1 inositol 1,4,5-trisphosphate receptor. *Nature* **379**, 168–171.

McKay BE & Turner RW (2005). Physiological and morphological development of the rat cerebellar Purkinje cell. *J Physiol* **567**, 829–850.

Michel V, Monnier Z, Guastavino JM, Propper A & Math F (2000). Functional alterations in the olfactory bulb of the *staggerer* mutant mouse. *Neurosci Lett* **280**, 1–4.

Miyata M, Kashiwadani H, Fukaya M, Hayashi T, Wu D, Suzuki T, Watanabe M & Kawakami Y (2003). Role of thalamic phospholipase Cβ4 mediated by metabotropic glutamate receptor type 1 in inflammatory pain. *J Neurosci* **23**, 8098–8108.

Miyazaki T, Fukaya M, Shimizu H & Watanabe M (2003). Subtype switching of vesicular glutamate transporters at parallel fibre-Purkinje cell synapses in developing mouse cerebellum. *Eur J Neurosci* **17**, 2563–2572.

Monnier Z, Bahjaoui-Bouhaddi M, Bride J, Bride M, Math F & Propper A (1999). Structural and immunohistological modifications in olfactory bulb of the *staggerer* mutant mouse. *Biol Cell* **91**, 29–44.

Nakagami R, Kohda K, Kakegawa W, Kondo T, Kato N & Yuzaki M (2008). Phosphorylation of δ2 glutamate receptors at serine 945 is not required for cerebellar long-term depression. *Keio J Med* **57**, 105–110.

Nakagawa S, Watanabe M, Isobe T, Kondo H & Inoue Y (1998). Cytological compartmentalization in the *staggerer* cerebellum, as revealed by calbindin immunohistochemistry for Purkinje cells. *J Comp Neurol* **395**, 112–120.

Nakao H, Nakao K, Kano M & Aiba A (2007). Metabotropic glutamate receptor subtype-1 is essential for motor coordination in the adult cerebellum. *Neurosci Res* **57**, 538–543.

Nicoletti F, Battaglia G, Storto M, Ngomba RT, Iacovelli L, Arcella A, Gradini R, Sale P, Rampello L, De Vita T, Di Marco R, Melchiorri D & Bruno V (2007). Metabotropic glutamate receptors: beyond the regulation of synaptic transmission. *Psychoneuroendocrinology* **32**(Suppl 1), S40–45.

Nusser Z, Mulvihill E, Streit P & Somogyi P (1994). Subsynaptic segregation of metabotropic and ionotropic glutamate receptors as revealed by immunogold localization. *Neuroscience* **61**, 421–427.

Park D, Lee S, Jun K, Hong YM, Kim DY, Kim YI & Shin HS (2003). Translation of clock rhythmicity into neural firing in suprachiasmatic nucleus requires mGluR-PLCβ4 signaling. *Nat Neurosci* **6**, 337–338.

Perkel DJ, Hestrin S, Sah P & Nicoll RA (1990). Excitatory synaptic currents in Purkinje cells. *Proc Biol Sci* **241**, 116–121.

Puro DG & Woodward DJ (1977). Maturation of evoked mossy fiber input to rat cerebellar Purkinje cells (II). *Exp Brain Res* **28**, 427–441.

Qiu CH, Shimokawa N, Iwasaki T, Parhar IS & Koibuchi N (2007). Alteration of cerebellar neurotropin messenger ribonucleic acids and the lack of thyroid hormone receptor augmentation by staggerer-type retinoic acid receptor-related orphan receptor-α mutation. *Endocrinology* **148**, 1745–1753.

Regehr WG, Carey MR & Best AR (2009). Activity-dependent regulation of synapses by retrograde messengers. *Neuron* **63**, 154–170.

Rich MM & Wenner P (2007). Sensing and expressing homeostatic synaptic plasticity. *Trends Neurosci* **30**, 119–125.

Sadakata T & Furuichi T (2009). Developmentally regulated Ca^{2+}-dependent activator protein for secretion 2 (CAPS2) is involved in BDNF secretion and is associated with autism susceptibility. *Cerebellum* **8**, 312–322.

Sadakata T, Kakegawa W, Mizoguchi A, Washida M, Katoh-Semba R, Shutoh F, Okamoto T, Nakashima H, Kimura K, Tanaka M, Sekine Y, Itohara S, Yuzaki M, Nagao S & Furuichi T (2007). Impaired cerebellar development and function in mice lacking CAPS2, a protein involved in neurotrophin release. *J Neurosci* **27**, 2472–2482.

© 2011 The Authors. Journal compilation © 2011 The Physiological Society

Safo PK, Cravatt BF & Regehr WG (2006). Retrograde endocannabinoid signaling in the cerebellar cortex. *Cerebellum* **5**, 134–145.

Sato K, Kiyama H & Tohyama M (1993). The differential expression patterns of messenger RNAs encoding non-N-methyl-D-aspartate glutamate receptor subunits (GluR1–4) in the rat brain. *Neuroscience* **52**, 515–539.

Serra HG, Byam CE, Lande JD, Tousey SK, Zoghbi HY & Orr HT (2004). Gene profiling links SCA1 pathophysiology to glutamate signaling in Purkinje cells of transgenic mice. *Hum Mol Genet* **13**, 2535–2543.

Serra HG, Duvick L, Zu T, Carlson K, Stevens S, Jorgensen N, Lysholm A, Burright E, Zoghbi HY, Clark HB, Andresen JM & Orr HT (2006). RORα-mediated Purkinje cell development determines disease severity in adult SCA1 mice. *Cell* **127**, 697–708.

Sidman RL, Lane PW & Dickie MM (1962). *Staggerer*, a new mutation in the mouse affecting the cerebellum. *Science* **137**, 610–612.

Sillevis Smitt P, Kinoshita A, De Leeuw B, Moll W, Coesmans M, Jaarsma D, Henzen-Logmans S, Vecht C, De Zeeuw C, Sekiyama N, Nakanishi S & Shigemoto R (2000). Paraneoplastic cerebellar ataxia due to autoantibodies against a glutamate receptor. *N Engl J Med* **342**, 21–27.

Sotelo C (1973). Permanence and fate of paramembranous synaptic specializations in "mutants" experimental animals. *Brain Res* **62**, 345–351.

Sotelo C (1975). Dendritic abnormalities of Purkinje cells in the cerebellum of neurologic mutant mice (*weaver* and *staggerer*). *Adv Neurol* **12**, 335–351.

Sotelo C (1990). Cerebellar synaptogenesis: what we can learn from mutant mice. *J Exp Biol* **153**, 225–249.

Sotelo C & Dusart I (2009). Intrinsic versus extrinsic determinants during the development of Purkinje cell dendrites. *Neuroscience* **162**, 589–600.

Staub C, Vranesic I & Knopfel T (1992). Responses to metabotropic glutamate receptor activation in cerebellar Purkinje Cells: Induction of an inward current. *Eur J Neurosci* **4**, 832–839.

Steinmayr M, Andre E, Conquet F, Rondi-Reig L, Delhaye-Bouchaud N, Auclair N, Daniel H, Crepel F, Mariani J, Sotelo C & Becker-Andre M (1998). *Staggerer* phenotype in retinoid-related orphan receptor alpha-deficient mice. *Proc Natl Acad Sci U S A* **95**, 3960–3965.

Takechi H, Eilers J & Konnerth A (1998). A new class of synaptic response involving calcium release in dendritic spines. *Nature* **396**, 757–760.

Tanimura A, Yamazaki M, Hashimotodani Y, Uchigashima M, Kawata S, Abe M, Kita Y, Hashimoto K, Shimizu T, Watanabe M, Sakimura K & Kano M (2010). The endocannabinoid 2-arachidonoylglycerol produced by diacylglycerol lipase alpha mediates retrograde suppression of synaptic transmission. *Neuron* **65**, 320–327.

Tehrani A, Wheeler-Schilling TH & Guenther E (2000). Coexpression patterns of mGLuR mRNAs in rat retinal ganglion cells: a single-cell RT-PCR study. *Invest Ophthalmol Vis Sci* **41**, 314–319.

Tempia F, Miniaci MC, Anchisi D & Strata P (1998). Postsynaptic current mediated by metabotropic glutamate receptors in cerebellar Purkinje cells. *J Neurophysiol* **80**, 520–528.

Vigh J, Li GL, Hull C & von Gersdorff H (2005). Long-term plasticity mediated by mGluR1 at a retinal reciprocal synapse. *Neuron* **46**, 469–482.

Vranesic I, Staub C & Knopfel T (1993). Activation of metabotropic glutamate receptors induces an outward current which is potentiated by methylxanthines in rat cerebellar Purkinje cells. *Neurosci Res* **16**, 209–215.

Weiss GM & Pysh JJ (1978). Evidence for loss of Purkinje cell dendrites during late development: a morphometric Golgi analysis in the mouse. *Brain Res* **154**, 219–230.

Yamakawa Y & Hirano T (1999). Contribution of mGluR1 to the basal activity of a mouse cerebellar Purkinje neuron. *Neurosci Lett* **277**, 103–106.

Yu J, Daniels BA & Baldridge WH (2009). Slow excitation of cultured rat retinal ganglion cells by activating group I metabotropic glutamate receptors. *J Neurophysiol* **102**, 3728–3739.

Yu LM & Goda Y (2009). Dendritic signalling and homeostatic adaptation. *Curr Opin Neurobiol* **19**, 327–335.

Yuan Q & Knopfel T (2006). Olfactory nerve stimulation-evoked mGluR1 slow potentials, oscillations, and calcium signaling in mouse olfactory bulb mitral cells. *J Neurophysiol* **95**, 3097–3104.

Zu T, Duvick LA, Kaytor MD, Berlinger MS, Zoghbi HY, Clark HB & Orr HT (2004). Recovery from polyglutamine-induced neurodegeneration in conditional SCA1 transgenic mice. *J Neurosci* **24**, 8853–8861.

Zucker RS & Regehr WG (2002). Short-term synaptic plasticity. *Annu Rev Physiol* **64**, 355–405.

Author contributions

All experiments were performed at Department of Neurophysiology, Gunma University Graduate School of Medicine. N.H. conceived and designed experiments. K.M. and N.H. performed the experiments and analysed the data. Interpretation of the data was done by N.H. N.F. and H.H. supervised the project. N.H. drafted the article and N.H. and H.H. revised it critically for important intellectual content.

Acknowledgements

We thank Noriyuki Koibuchi for providing us with *staggerer* mutant mice, Chiho Koyama for technical assistance with Western blot, Yumiko Iwazaki for technical assistance with immunohistochemistry, and Makiko Iguchi for maintaining and genotyping the mutant mice. We thank Junichi Hitomi for sharing quantitative PCR data. This project was supported in part by a Grant-in-Aid from the Japan Society for the Promotion of Science (JSPS), MEXT; grants from Research on Measures for Intractable Diseases (Ataxic Diseases and Neurodegenerative Diseases) from the Ministry of Health, Labour and Welfare, the Sumitomo Foundation, Takeda Science Foundation and Uehara Memorial Foundation (to H.H.).

© 2011 The Authors. Journal compilation © 2011 The Physiological Society